Clim. Past Discuss., 9, 2717–2770, 2013
www.clim-past-discuss.net/9/2717/2013/
doi:10.5194/cpd-9-2717-2013

Climate of the Past Discussions
Open Access

Dynamic soil feedbacks on the climate of the mid-Holocene and the Last Glacial Maximum

M. Stärz[1,2,3], G. Lohmann[1,4], and G. Knorr[1]

[1]Alfred Wegener Institute Helmholtz Centre for Polar and Marine Research, Bremerhaven, Germany
[2]Senckenberg Research Institute and Natural History Museum, Frankfurt/Main, Germany
[3]Biodiversity and Climate Research Centre (LOEWE BiK-F), Frankfurt/Main, Germany
[4]University of Bremen, Bremen, Germany

Received: 7 May 2013 – Accepted: 9 May 2013 – Published: 24 May 2013

Correspondence to: M. Stärz (michael.staerz@awi.de)

Published by Copernicus Publications on behalf of the European Geosciences Union.

Abstract

State-of-the-art general circulation models (GCMs) are tested and challenged by the ability to reproduce paleoclimate key intervals. In order to account for climate changes associated with soil dynamics we have developed a soil scheme, which is asynchronously coupled to a state-of-the-art atmosphere ocean GCM with dynamic vegetation. We test the scheme for conditions representative of a warmer (mid-Holocene, 6 kyr before present, BP) and colder (Last Glacial Maximum, 21 kyr BP) than pre-industrial climate. The computed change of physical soil properties (i.e. albedo, water storage capacity, and soil texture) for these different climates leads to amplified global climate anomalies. Especially regions like the transition zone of desert/savannah and taiga/tundra, exhibit an increased response as a result of the modified soil treatment. In comparison to earlier studies, the inclusion of the soil feedback pushes our model simulations towards the warmer end in the range of mid-Holocene studies and beyond current estimates of global cooling during the Last Glacial Maximum based on PMIP2 (Paleoclimate Modelling Intercomparison Project 2) studies. The main impact of the interactive soil scheme on the climate response is governed by positive feedbacks, including dynamics of vegetation, snow, sea ice, local water recycling, which might amplify forcing factors ranging from orbital to tectonic timescales.

1 Introduction

As yet climate sensitivity on long timescales is still underestimated by General Circulation Models (GCMs) (e.g. Pagani et al., 2010; Valdes, 2011). Proxy records from the hothouse tectonic past (late Cretaceous, Cenozoic) indicate a decreased meridional global temperature gradient with amplified warming in polar regions known as equable climate (Jenkyns et al., 2004; Moran et al., 2006; Huber and Caballero, 2011; Salzmann et al., 2013). Apart of high atmospheric CO_2-levels, plausible mechanisms have been proposed (polar stratospheric clouds, vegetation dynamics, oceanic heat

CPD
9, 2717–2770, 2013

transport, orbital parameters), trying to fit models towards proxy data (Sloan et al., 1995; Otto-Bliesner and Upchurch, 1997; Sloan and Morill, 1998; Sloan and Pollard, 1998; Kump and Pollard, 2008; Willeit et al., 2013).

Another potential mechanism is pedogenesis, which is not yet accounted for in present earth system models with land surface dynamics. In general soil genesis is controlled by time, parent material, topography, climate, vegetation (and humankind) (Jenny, 1941). So far general circulation models (GCMs), trained to simulate present and thus future climate scenarios for the next ∼ 100–300 yr (Meinshausen et al., 2011), do not account for soil development. Typically pedogenesis is operating in the range of 100–1000 yr and more (Jenny, 1941), but degradation of soils by erosion due to land cover change like deforestation can happen on much shorter timescales. For instance it has been speculated, if intensive land use and thus the exposure of bright underlying soils in the Sahel zone triggered the inter-decadal drought event ∼ 1969 (Nicholson et al., 1998). In analogy to modern climate, the Sahel also has been undergone a dramatic desertification during the mid-Holocene 5500 yr ago (Foley et al., 2003). A rather immediate change from humid mid-Holocene conditions to desertification of Sahel by gradual change of orbital parameters calls for strong nonlinearities in the Sahel climate system.

Many modeling studies have investigated the intensification of Holocene wind systems in North Africa (e.g. Kutzbach and Otto-Bliesner, 1982; Kutzbach and Street-Perrott, 1985; Kutzbach and Guetter, 1986; deMenocal and Rind, 1993) resulting in decreased Sahara desert area and a northward shift of the Sahel. Evidence is retrieved by various proxy records, like abundance of pollen data in marine (Dupont, 2011) and terrestrial archives (Prentice et al., 2000; Bartlein et al., 2011), paleolakes (Petit-Maire and Riser, 1981; Hoelzmann et al., 1998, 2000), human migration and inhabitation (Petit-Maire, 1989), skeletal remnants of herbivores (Petit-Maire and Riser, 1981; Petit-Maire, 1989) and rock engravings (McIntosh and McIntosh, 1983). The cause for this impact is supposed to be increased seasonal contrast of solar radiation (and higher insolation in the northern high latitudes, Berger, 1978) since atmospheric

CPD
9, 2717–2770, 2013

greenhouse gases were close to pre-industrial values (Petit et al., 1999). Basically the concept of fast land surface heating compared to the inertia of the ocean during the spring to summer transition results in inland moisture convergence and strong precipitation events. Based on the theory of land to ocean contrast (Charney, 1975; Charney et al., 1977) model studies with modified earth's orbit gradually investigated the influential impact of increased Atlantic SSTs (e.g. Kutzbach and Liu, 1997; Texier et al., 2000; Zhao et al., 2005), feedbacks by vegetation migration (Kutzbach et al., 1996; Texier et al., 1997, 2000; Claussen, 1997; Claussen and Gayler, 1997; Braconnot et al., 1999, 2007), enhanced land evapotranspiration through higher abundance of lakes and wetlands (Coe and Bonan, 1997; Broström et al., 1998; Carrington et al., 2001; Krinner et al., 2012) and increased water holding field capacities in soils (Levis et al., 2004) and decreases in land surface albedo (Bonfils et al., 2001; Levis et al., 2004; Knorr and Schnitzler, 2006; Schurgers et al., 2007; Vamborg et al., 2011) on the moisture bearing African wind system. Actually, numerical models taking into account integrated atmosphere-ocean-vegetation feedbacks are evaluated to represent the mid-Holocene African monsoon more realistically (Braconnot et al., 2007).

Several studies have raised the role of pedogenesis influencing land surface energy balance, water re-cycling and thus vegetation impact, which might be crucial for Holocene climate simulations as well as for future climate scenarios or on tectonic timescales (Kutzbach et al., 1996; Doherty et al., 2000; Levis et al., 2004; Knorr and Schnitzler, 2006; Shellito and Sloan, 2006; Wanner et al., 2008; Brovkin et al., 2009; Micheels et al., 2009; Knorr et al., 2011; Krapp and Jungclaus, 2011; Vamborg et al., 2011). Furthermore, model studies testing the sensitivity of land surface albedo highlight the importance to achieve not only for vegetation dynamics but also for background albedo (Kutzbach et al., 1996; Levis et al., 2004; Knorr and Schnitzler, 2006; Jiang, 2008). Recently, Vamborg et al. (2011) for instance, successfully integrated dynamically computed foliage litter in a GCM with dynamical vegetation, which dims land surface albedo and hence strengthens mid-Holocene African wind system. Apart from that, present-day studies highlight the importance of soil moisture feeding back to

CPD
9, 2717–2770, 2013

precipitation (e.g. Bergengren et al., 2001; Douville et al., 2001, 2007) and modulating local seasonal precipitation (e.g. Seneviratne et al., 2006, 2010). In an atmospheric GCM study Wang (1999) associated finer soil texture and darker soils with vegetation reconstructions of the mid-Holocene, resulting in intensified East Asian rainfall and improved quantitative agreement to proxy records. In addition to changes in soil albedo, Levis et al. (2004) isolate the effect of modified soil texture from desert sand to loam which increases soil water retention. They find a weak but widespread increase of evapotranspiration at Sahara but North African rain belt is dominated by modified land albedo. Continuatively Jiang (2008) investigated the role of physical soil characteristics (soil colour, soil texture) for the Last Glacial Maximum by using an atmospheric GCM asynchronously coupled to a terrestrial biosphere model. In his procedure he iteratively adapted soil characteristics if absolute simulated vegetation in a grid cell has changed. The integrated vegetation-soil feedback reinforced glacial cooling to some extent (Jiang, 2008).

The advent of coupling vegetation with climate models was initiated by Henderson-Sellers (1993) and Claussen (1994). As a starting point Henderson-Sellers (1993) used a version of the Holdridge (1947) Life zone classification, condensed it to ten different continental vegetation classes, thereby these were translatable to ecotypes of the Biosphere-Atmosphere Transfer Scheme and coupled it with the atmospheric model CCM1 (Williamson et al., 1987). In a parallel approach Claussen (1994) used the equilibrium vegetation model BIOME1 by Prentice et al. (1992) and applied an asynchronous coupling technique with the AGCM ECHAM3 (Roeckner et al., 1992). Therein ECHAM3 computes climate data fields which are passed to BIOME1 to calculate equilibrium plant distribution. Subsequently the physical parameters of simulated vegetation types are handed back to the atmosphere model for restarting initialisation. This procedure is iteratively repeated until vegetation and climate model are equilibrated (Claussen, 1994). After recognising its importance, dynamical vegetation models became fully integrated into GCMs (e.g. Foley et al., 1994, 2000).

CPD
9, 2717–2770, 2013

Here we introduce a simple equilibrium soil scheme, asynchronously coupled to COSMOS-ASO, alike the procedure of Claussen (1994). The purpose is to capture biogeophysical feedbacks between soil genesis/degradation and climate (COSMOS-ASO_{sol}) as proposed by Levis et al. (2004). The effect of the soil feedback is tested in model setups representing a warm (mid-Holocene) and cold (Last Glacial Maximum) climate relative to Pre-industrial and compared to geological data to set a range of potential soil impact on global climate for glacial and interglacial periods of the Quaternary.

2 Methods

2.1 Model description

In the current model setup, we use three model components (atmosphere, ocean, land surface) coupled to each other within the COSMOS model suite (community of earth system models). The atmospheric component is represented by ECHAM5 (Roeckner et al., 2003) with a spectral resolution of T31L19 (3.75°) which is an adequate compromise in terms of CPU time for longer simulation length (Roeckner et al., 2006). The ocean model MPI-OM uses an orthogonal curvilinear grid (~1.5°) with higher resolution at deep water formation areas of Labrador Sea and Weddel Sea near the grid poles (Greenland, Antarctica) and 40 layers in vertical space (Marsland et al., 2003). The transfer of fluxes and momentum between atmosphere and ocean is handled by the coupler OASIS3 without any flux corrections (Jungclaus et al., 2006). The modular land surface scheme JSBACH (Raddatz et al., 2007) with dynamic vegetation (Brovkin et al., 2009) is embedded in the ECHAM5 atmosphere model. JSBACH is based on the semi-empirical terrestrial ecosystem model BETHY, which incorporates an energy and water balance, photosynthesis, phenology (not used in our approach because of dynamic vegetation) and a carbon balance compartment (Knorr, 2000). JSBACH is using a tiling approach in which the actual cover fraction of each plant functional type (PFT)

CPD
9, 2717–2770, 2013

is associated to a tile for each grid cell. If the grid cell is not fully covered by the sum of all tiles, the residual is interpreted as bare soil. In our studies JSBACH is using the standard model configuration of eight PFTs which can potentially cover each grid cell. The land surface energy balance incorporates soil albedo, leaf area index of the actual PFT, the albedo of stems, snow fraction on the ground and on canopy and the masking effect of snow under canopy. Further background information of the COSMOS model suite and its components can be found in Jungclaus et al. (2006). So far COSMOS has been applied to various paleo setups like Holocene (Wei et al., 2012; Wei and Lohmann, 2012; Varma et al., 2012), Last Glacial Maximum and MIS3 (Zhang et al., 2012; Gong et al., 2013), Last Interglacial (Lunt et al., 2013), Pliocene (Stepanek and Lohmann, 2012) and Tortonian (Knorr et al., 2011).

2.2 Design of the soil scheme

In our concept pedogenetic factors like climate and topography are indirectly captured by simulated vegetation distribution whereas parent material is ignored. Physical soil properties like albedo are dependent on the accumulation of organic matter and therefore of the specific vegetation type above (e.g. Vamborg et al., 2011). Moreover, observational data to total water holding field capacities of soils are limited and tuned to optimized rooting depths in order to fit to vegetation demands (Hagemann et al., 1999). In our approach these soil parameters are evaluated by integrated PFTs of each grid cell by the dynamic land surface model JSBACH (Fig. 1). For each grid cell the contribution of all area-weighted soil tiles creates a mean of soil characteristics.

All time-slice experiments start from a quasi-equilibrium climate state and the first iteration uses a mean of 100 yr model output to calculate physical soil properties (soil albedo in the spectrum of visible and near-infrared light, soil data flags FAO, maximum water holding field capacity of soils). After the first iteration the model is run for 600 yr in total with an asynchronous coupling time step of 200 yr, again taking the preceding 100 yr of model output as input for the soil scheme (Fig. 1). The final 100 yr of model output and physical soil characteristics of the 3rd iteration are used for analysis.

CPD
9, 2717–2770, 2013

2.3 Look-up table of physical soil characteristics

Soil parameters in JSBACH comprise the snow free soil albedo in the visible (0.3–0.7 µm) and near infrared (0.7–3 µm) light spectrum, the total water holding capacity of soil (W_{cap}) and soil data flags from the United Nations Food and Agriculture Organization (FAO) soil classification (Hagemann et al., 1999; Hagemann, 2002; Rechid et al., 2009). The original dataset of snow free soil albedo is derived from modified satellite measurements of the Moderate Resolution Imaging Spectroradiometer (MODIS) (Rechid et al., 2009). FAO soil data flags based on Gildea and Moore refer to Henderson-Sellers et al. (1986), and range from sand (1) to loam (3) and clay (5). The assessment of h_{cws} in global and regional modeling is quite uncertain and is estimated by a dataset of the parameter h_{pwp} (permanent wilting point) and h_{ava} (maximum amount of water that plants may extract from the soil before they start to wilt) based on optimized rooting depths (Hagemann et al., 1999).

In our model consistent approach the association of soil properties to PFTs is developed using the last 100 yr output of a 2000 yr pre-industrial equilibrium model run (Wei et al., 2012). The main properties of defined soil tiles are displayed in its latitudinal distribution (Fig. 2). Only dominant cover fractions of modeled PFTs (< 50 % cover per grid cell) are considered to create associated soil tiles. This approach is extended by adding soil tiles for global desert fraction (defined by the fraction of a grid cell not covered by any vegetation for at least 50 yr) and a parameterization for the Arabian Peninsula/Sahara desert region in order to consider extremes of h_{cws} and soil albedo of bare soils identified in Fig. 2 (yellow crosses). Furthermore we discriminate globally distributed C3 grasses to "warm" (> 0 °C mean annual temperature, MAT) and "cold C3 grasses" (< 0 °C MAT) to account for a more realistic climate sensitivity. The simulated PFT "cold shrubs" does not exceed cover fractions more than 50 % and therefore it is ignored in the calculation. Since cold shrubs are always associated to grid cells dominated by "cold C3 grasses", we combined both classes to one soil tile anyway. The adjusted classification of physical soil characteristics is shown in Fig. 2. Calculated

CPD
9, 2717–2770, 2013

means of the dataset are summerized in Table 1. In general desert soil tiles show low water holding field capacities and high soil albedo. C4 perennial grasses also have relative high soil albedo and maximum field capacities of water due to high rooting depth. Soil tiles associated to tropical canopy are in the medium range of soil albedo and at the upper range of total water holding field capacities. Soil tiles of temperate/boreal forest, typically located at mid and high northern latitudes have relative low soil albedo (Fig. 2, Table 1), where land albedo increases with increasing leaf area index (LAI) during summer months (Rechid et al., 2009). The FAO soil data flags (refers to Gildea and Moore, in Henderson-Sellers et al., 1986) are a coarse classification of soil texture and are indifferent due to our soil tiles. The calculated mean in soil texture is loam (3) for all soil tiles except for "tropical broadleaved evergreen forest" where a more fine mixture of loam and clay (4) is associated to. By calculation of means, extremes of physical soil properties vanish; therefore we conclude the constructed lookup-table of physical soil tiles is rather a conservative estimate.

2.4 Soil scheme

The soil scheme computes the actual soil tiles n consistent to the procedure described in Sect. 2.3. Then soil properties sol_n (h_{cws}, fao, $\alpha_{\mathrm{s,vis}}$, $\alpha_{\mathrm{s,nir}}$) referring to the lookup-table (Table 1) are calculated by a vegetation index. The vegetation index weights the cumulative cover fraction of soil tiles f_i per grid cell:

$$\mathrm{sol}_n = \frac{\sum_{i=1}^{11} (f_i \mathrm{sol}_i)}{\sum_{i=1}^{11} f_i} \quad (1)$$

Grid cells affected by the Arabian Peninsula/Sahara desert parameterization (Sect. 2.2) are not weighted by the procedure. The Arabian Peninsula/Sahara desert parameterization is defined by grid cells of at least 50 % desert coverage between a latitudinal

CPD
9, 2717–2770, 2013

belt (13–35.26° N). We use a sill value of 50 % desert fraction for a better representation of the Sahel (desert/savannah) transition zone where vegetation cover is generally overestimated by JSBACH (Vamborg et al., 2011).

2.5 Experimental design

In this study three reference runs are taken, a pre-industrial PI_ctl (Wei et al., 2012), a relatively warm climate state for mid-Holocene (HOL, 6 ka before present) HOL_ctl (Wei et al., 2012) and a model run representing the Last Glacial Maximum (LGM ~ 19 ka BP) colder than present day LGM_ctl (Zhang et al., 2012), all performed by the conventional COSMOS-ASO configuration. The reference runs follow the setup procedure of the Paleoclimate Modelling Intercomparison Project PMIP2 (Braconnot et al., 2012) and run into adjusted equilibrium. The setup of HOL_ctl uses a different orbital parameter configuration and methane concentration in the atmosphere of 650 instead of 760 parts per billion compared to Pre-industrial (Wei et al., 2012). Adjustments of boundary conditions for LGM include orbital parameters, sea-level drop and coherent ice-sheet extent, elevation and an initial salinity increase of the glacial ocean by 1. Apart from the PMIP2 considerations land-sea mask and ocean gateways are typically tuned and LGM_ctl is initialized from a glacial ocean which lead to a more realistic glacial ocean circulation (Zhang et al., 2012). The length of model the simulations PI_ctl as well as HOL_ctl are 3000 yr whereas LGM_ctl is run for 5400 yr in total. The last model year of each reference run is used for initialization of our soil experiments and run for another 600 yr in total.

The impact of the soil scheme on climate (HOL, LGM) is examined using the factor separation technique used for identifying synergies in numerical models by Stein and Alpert (1993) in order to disentangle the effect of soil and climate (HOL_sol-PI_sol and LGM_sol-PI_ctl, respectively) by subtracting the single contribution of climate. Here the effect of soil under warmer/cooler climate is indicated by $\widehat{f}_{i,\mathrm{sol}}$:

CPD
9, 2717–2770, 2013

$$\widehat{f}_{i,\mathrm{sol}} = (\mathrm{sol}_i - \mathrm{PI\_sol}) - (\mathrm{ctl}_i - \mathrm{PI\_ctl}) \quad (2)$$

soil feedback = (climate and soil) – climate

where the index i represents the respective climate state (LGM, HOL). Further, this procedure cancels out the error of routine by including the soil scheme (PI_sol-PI_ctl). We have to assume that the magnitude of error of routine, calculated for Pre-industrial is the same as in our paleo simulations.

3 Results

3.1 Pre-industrial simulation

In Fig. 3 global surface air temperature, precipitation and evaporation anomalies of PI_sol-PI_ctl are shown. At high northern latitudes surface air temperatures are locally increased about 1 °C at the Canadian Archipelago and Baffin Bay affected by reduced sea-ice cover in consequence of a change in soil characteristics. In general reduced sea-ice cover is observed in areas around the coasts encapsulating the Arctic Ocean and Barents Sea as well as the Antarctic continent. The Arabian Peninsula/Sahara desert parameterization exhibit anomalies in the surface radiation balance which are related to deviations in land albedo compared to the original input-file of PI_ctl. The soil albedo directly reflects a temperature signal because of the absence of vegetation cover in this area. Regional temperature anomalies vary from −3.2 °C (desert regions in South Asia) to +2.3 °C (Sahara desert) where land albedo are over- (+0.14) or underestimated (−0.08), respectively. The surface of the Southern Ocean is warming due to reduced sea-ice cover and a decrease in strength of the Atlantic Meridional Overturning Circulation (AMOC) which is accompanied by less heat advection from the South. Here the AMOC is reduced by 1 Sv ($1\,\mathrm{Sv} = 1 \times 10^6\,\mathrm{m^3\,s^{-1}}$) compared to the pre-industrial run (16 Sv). In Fig. 3b total precipitation shows some regional anomaly

CPD
9, 2717–2770, 2013

patterns in lower latitudes, i.e. an anomalous northward shift of the Indonesian rainfall, and increased precipitation in tropical rainforests. A similar pattern is observed in the evaporation anomaly (Fig. 3c). In general the global pattern of water holding field capacities is reasonably captured by our simulation (not shown), thus underestimating maximum values in the tropics and east of china by our soil lookup-table (Table 1). The soil scheme overestimates field water capacities in North Europe and North America where soil progression is lagged by deglacial ice sheet retreat. Since there is no time-dependent function of soil evolution in our soil scheme, our model exhibits an equilibrated final state of the physical soil characteristics in these regions. Globally the water holding field capacity of soil becomes higher (+0.06 m) than PI_ctl (0.63 m) but the global inventory of soil water is slightly reduced (−0.008 m). Further, evaporative processes over land increase (+0.012 mm day^{-1}) and land surface runoff and drainage is increased (+0.014 mm day^{-1}) but compensated by the atmospheric exchange of fluxes via total precipitation over land (+0.027 mm day^{-1}). The global mean of surface air temperature is increased by +0.27 °C.

In PI_sol the simulated forest cover slightly increases in high latitudes and decreases in subtropical regions where it is replaced by grass cover (Fig. 3d and e). The inclusion of the soil scheme particularly favors the expansion of forests by reduced temperatures of the coldest month especially in the northeast of Canada, Canadian Archipelago (2–5 °C) and North Siberia (∼ 1 °C). In the subtropical areas grass cover increases to the expense of forest cover mainly due to an underestimation of the calculated water field capacity of soils in the soil scheme.

3.2 Mid-Holocene climate

The mid-Holocene simulation HOL_sol is characterized by a redistribution of solar radiation caused by modified settings of the orbital parameters and a reduced level of methane content in the atmosphere (650 parts per billion) compared to CTL_sol which leads to an overall warming of +0.34 °C. Most of the warming anomaly can be found in high northern latitudes especially in the Barents Sea (> 7 °C), where sea ice retreats

CPD
9, 2717–2770, 2013

(Fig. 4). A moderate warming of ∼ 1 °C is observed in the tropics as well as some local areas of Sahara and Arabian Peninsula. Regional cooling from −1 to −3 °C is located in typical monsoon regions like Sahel and India. The precipitation anomaly (Fig. 5) confirms that land surface cooling occurs in areas of high land precipitation and evaporation (Fig. 6) consistent with increased latent heat fluxes. The northward shift of the precipitation anomaly causes reduced rainout above Brazil, South Africa and Australia, thus decreasing tropical forest cover there (Fig. 7). Therefore reduced evapotranspiration in the tropics results in a warming anomaly in consequence of less latent heat transfer.

The mid-Holocene land surface is described by higher occurrence of forests (+2.6 %) in expense of grassland and a decline in the desert fraction (−4.4 %). In more detail trees are more abundant in North Canada and North Siberia as well as Sahara/Sahel boundary, but reduced in some other regions, in Europe for instance. Nevertheless grass cover increases in total (+0.8 %) especially in the Sahara, whereas desert reduces at the southern boundary of the Sahara and in high northern latitudes. Since terrestrial vegetation beyond Sahara/Sahel does not exceed 50 %, adaption of soil characteristics is not applied (see Sect. 2.3).

3.3 LGM climate

Modified earth's orbital configuration, adapted greenhouse gas concentrations in the atmosphere, expansion of the LGM ice sheets in height and surface area as well as a sea level drop, following the protocol of PMIP2, lead to a subsequent global surface cooling of −7.03 °C. Strongest cooling is located at the peak of ice sheets and Nordic Seas, where perennial sea-ice cover evolve (Fig. 4). The impact of the introduced soil scheme results in an additional cooling of −1.07 °C with highest anomalies in high northern latitudes and some regional cooling anomalies at subtropical land surface spots. In the atmosphere the absolute air humidity is strongly reduced thus dampening evaporation (Fig. 6) and precipitation (Fig. 5) in a glacial climate. Total precipitation decrease at the equator in the inner tropical convergence zone and latitudes > 40° in global mean by

CPD
9, 2717–2770, 2013

$-0.42\,\mathrm{mm\,day^{-1}}$. The expansion of sea-ice cover towards the equator reduces water vapour transport to the poles, forcing a rainout along the horse latitudes (~ 30° N, S) where total precipitation is increased (Fig. 5). The terrestrial vegetation show a decrease of forest cover (−14.9 %) compensated by grass cover (+10 %) and expansion of polar and Sahara desert area (+12.7 %). Taken the additional area of exposed shelf seas into account, trees (+6 % in global mean) and grasses (+7 %) can evolve there. Major retreat in boreal forest cover arises in Eurasia in a zonal belt between 50–65° N and at the proximity of Scandinavian and Laurentide ice sheet (Fig. 8). Interestingly, forest cover slightly increases along the horse latitudes in response to higher precipitation there. Tropical forest cover is dramatically reduced by −59 % compared to PI_sol. In most areas grass cover compensates for forest regression. Nevertheless, in areas affected by desert expansion, e.g. Arabian Peninsula, Sahara/Sahel borderline and North Siberia, grassland disappears and bare soil remains.

3.4 Dynamic physical soil characteristics and their impact on mid-Holocene and LGM climate

Computed changes of soil albedo and water holding field capacities by the soil scheme under different climate states are shown in Fig. 9. The soil scheme discriminates soil texture (five types, ranging from clay to sand) only into two types, loam-and-clay under prevailing tropical broadleaved evergreen forest and loam for the residual land surface. For a warmer than pre-industrial climate the global mean field capacity of soil increases by +0.024 m over land surfaces (without ice sheet) especially at the Sahel, transition zone of desert and savannah. Consequently the global soil water body increases by +0.019 m compared to PI_sol (Fig. 10). The synergetic term of soils and mid-Holocene climate exhibit an increase of soil wetness of +0.013 m in global mean (Table 2). Further an increase of landward water transport ($+1.29\,\mathrm{kg\,m^{-2}\,yr^{-1}}$) from the ocean, land surface runoff and drainage ($+3.35\,\mathrm{kg\,m^{-2}\,yr^{-1}}$) is affected by changes of physical soil properties.

CPD
9, 2717–2770, 2013

The global mean of land surface albedo decreases by −0.011, with maximum anomalies > 0.19 at the Sahel region caused by vegetation migration towards the Sahara where it shades the modified soil albedo (Fig. 4). The integrated zonal mean of high northern latitude land albedo decreases due to a darkening of the soil (Fig. 9) accompanied by increased forest cover (Fig. 7) and less snow cover (Fig. 11). Forest cover replaces C3 grass cover and thus modifies soil characteristics: Higher abundance of boreal evergreen forest in high latitudes leads to a lowering of the soil albedo and higher maximum water holding field capacities compared to soils associated to C3 grasses. Darker soils are generated leading to a change in the local energy budget and higher surface air temperatures arise which in turn lead to an amplified decrease of polar desert cover, again reinforcing soil genesis (see Sect. 3.4.2).

The computed soil characteristics of the LGM model simulation show a global decrease in water holding field capacities (Fig. 9b), which is overcompensated by soil formation at exposed shelf seas, added to land surface grid cells (Table 2). This variable strongly modulates soil wetness (Fig. 10b). Along a zonal mean the soil albedo increases, especially in high latitudes (Fig. 9b). In consequence, calculated land surface albedo also increases, especially in Asia and in the vicinity of expanding desert areas (Fig. 10d) due to the expense of grass and forest cover there (Fig. 8).

3.4.1 Water cycle

A change in physical soil characteristics like water field capacity in soils potentially impacts the hydrological cycle over land. The mid-Holocene model simulation with dynamic geophysical soil characteristics shows increased evaporation over land surface areas contributed by additional moisture flux from the ocean towards land (Table 2). Higher land evaporation is supported by an increase in temperature and transpiration of forest (+2.6 %) and grass cover (+0.8 %) change. Consequently, elevated land precipitation and soil moisture result in increased drainage and land surface runoff. The soil scheme amplifies each of the described processes in the water cycle, but favors forest cover (+0.9 %) instead of grassland (−0.6 %) (Fig. 7).

CPD
9, 2717–2770, 2013

The mid-Holocene configuration of orbital parameters results in stronger seasonal amplitudes of solar radiation. After winter period, when solar radiation increases, a land to ocean temperature contrast evolves, caused by the thermal inertia of the ocean relative to land surface. The land/ocean temperature gradient favors moisture transport towards inland, as seen in the African monsoon for instance. This mechanism is intensified by the setting of orbital parameter configuration during the mid-Holocene, when summer solstice was closer to perihelion of earth's orbit. In general this can be seen in a net water vapor transport from ocean towards land compared to ctl_sol (Table 2). An intensification of the African wind system leads to increased precipitation in the Sahel zone favouring the establishment of forest cover. Also in high northern latitudes, where sea-ice cover is reduced due to warmer temperatures, more open waters contribute to increased evaporation over ocean (e.g. Barents Sea). Therefore global forest cover can increase and expand in areas formerly characterized by tundra (C3 grasses and cold shrubs) or desert. The resulted change of terrestrial vegetation cover lead to higher water storage capacities in soils (Table 2), typically found under forests and C4 grasses and thus, as a result, soils moisten. In consequence of extended forest cover and higher temperatures, land evaporation (and transpiration) and precipitation increase significantly, amplified by the effect of higher water storage in soils (Table 2). In HOL_sol the additional atmospheric water transport from ocean to land together with land precipitation is not fully compensated by evaporation, closing the hydrological cycle via elevated drainage and land surface runoff towards the ocean (Table 2).

In a glacial climate regime like LGM, with significantly colder surface temperatures than Pre-industrial (−7.03 °C), land evaporation and net water transport from ocean towards land is reduced. All forest PFTs and C4 grasses retreat due to unfavorable climate conditions and are replaced by shrubs and grassland reducing evapotranspiration. The synergetic effect of a cold, dry climate and soil formation leads to a subsequent degradation with lower soil water storage capacities (−7.05 cm) resulting in decreased soil wetness (−4.5 cm) and increased surface runoff (+2.62 $kg\,m^{-2}\,yr^{-1}$). However, LGM_sol is characterized by higher soil water storage capacity and soil water

CPD
9, 2717–2770, 2013

content compared to PI_sol. This can be explained by the sea-level drop, which expose ocean to land surface grid points, especially in shelf areas of Arctic Ocean and Indonesian Archipelago. Climate conditions and additional vegetation cover in low latitudes favor soil formation processes in the exposed ocean grid points, therefore anomalies of maximum field water capacities (Fig. 9) in the tropics exhibit highest anomalies compared to high latitude grid cells (Fig. 10). In consequence the overall decrease of maximum water storage capacities in soils (−8.76 cm) is overcompensated by the additional land surface grid points leading to wetter soils (+3.03 cm).

3.4.2 Heat balance and surface air temperatures

Global mean of total incoming radiation for the mid-Holocene simulation is slightly reduced compared to the pre-industrial control run ($-0.14\,W\,m^{-2}$). Nevertheless the configuration of orbital parameters results in a redistribution of incoming solar radiation from the tropics into the high latitudes. In consequence of nonlinearities in the climate system, feedback mechanisms acting especially in high latitudes, HOL_sol gets comparably warmer (+0.34 °C) than CTL_sol. More shortwave radiation ($-2.88\,W\,m^{-2}$) at the surface is transferred to longwave radiation ($+2.49\,W\,m^{-2}$) by a darkening in land surface albedo (without consideration of Greenland and Antarctic ice sheet) which results in a warming of the mid-Holocene simulation. This is partly compensated by the transfer of energy via latent heat flux ($+2.06\,W\,m^{-2}$) which can lead to regional cooling, where latent heat flux is bigger than sensible heat flux, for instance in the southern Sahel region. The synergetic effect of physical soil properties and climate amplify the warming during the mid-Holocene epoch of about ∼ 70 % (+0.24 °C) in our model simulations especially at the land surface (+0.44 °C). The increased soil water storage capacities at the Sahel region and high northern latitudes increase the soil water content, fostering evaporation (see Sect. 3.4.1) and cooling due to stronger latent heat transfer ($+0.29\,W\,m^{-2}$). Anyway, sensible heat flux shows a higher transfer of energy ($+0.71\,W\,m^{-2}$) to temperature via changes of soil albedo which overcompensate latent heat transfer. Affected regions can be found in transitional climate regimes

CPD
9, 2717–2770, 2013

characterized by positive changes in vegetation cover with bare soil (Fig. 7) like Northern Siberia and northern Sahel zone. In the north-polar region an increase in forest cover as seen in the anomaly plot (Fig. 7a) and the synergy of soil processes (Fig. 7b) leads to a shading of the snow cover beneath the forest canopy, a darkening of the albedo resulting in higher sensible heat flux at the surface. Including physical soil properties tend to amplify this process by earlier spring snow melt due to the surrounding of darker soils with an anomalous increase in spring temperatures as a consequence. This mechanism act in concert with a delayed expansion of sea-ice cover (initiated by the stronger insolation at the poles and enlarged seasonal insolation contrast of orbital parameter setting) during autumn which further decreases the planetary albedo. With the retreat of sea-ice cover the insulation effect between atmosphere and ocean disappears and the heat flux increases. Both mechanisms tend to enlarge the growing season of terrestrial vegetation.

The model simulation of the Last Glacial Maximum (LGM_sol) is characterized by increased snow cover, a retreat of tropical forest cover (−59 % compared to PI_sol) and expansion of Sahara desert, a southward shift of the boreal tree line to ∼ 58° N and a replacement from tundra to polar desert in North Siberia (Fig. 8) which raise land surface albedo. The synergetic effect of a glacial climate and adaptable geophysical soil parameters exhibit an amplified decrease in forest cover (−2.6 %) substituted by grassland (+2.7 %) and expansion of desert regions (+1.4 %). This leads to a brightening of the land surface (Fig. 9b) and increased backscattering of shortwave radiation ($+7.09\,W\,m^{-2}$) supported by changes of geophysical soil properties ($+2.52\,W\,m^{-2}$). In consequence of the cooling and the decrease of terrestrial vegetation evapotranspiration is reduced. Therefore latent heat flux is strongly reduced ($-4.15\,W\,m^{-2}$) corroborated by the effect of degraded water holding field capacities in soils ($-1\,W\,m^{-2}$). This effect decreases the most in a zonal belt between 50–65° N over Asia, where tree cover is drastically reduced and soil characteristics have changed. The migration of forests exposes brighter degraded soils compared to PI_ctl and sensible heat flux is reduced as well in consequence.

CPD
9, 2717–2770, 2013

If the evolution of additional land surface area in consequence of sea-level drop is taken into account, the effect of latent and sensible heat transfer is attenuated or even reversed (+4.4 $W m^{-2}$). Nevertheless compared to evaporation over substituted open ocean waters (−656 $kg m^{-2} yr^{-1}$) this effect is negligible.

4 Discussion

4.1 Dynamic soil feedback for the mid-Holocene climate

Considering the dynamic adaptation of physical soil characteristics, our results indicate a warmer mid-Holocene climate than shown in most previous modelling studies with dynamic vegetation (Gallimore et al., 2005; Braconnot et al., 2007; Otto et al., 2009a,b). Global surface air temperatures of +0.34 °C in our simulation are comparable with a mean warming of +0.36 °C in the study of O'ishi and Abe-Ouchi (2011) using a GCM with slab-ocean-atmosphere-vegetation dynamics. They state that most of their warming is derived from vegetation dynamics (+0.23 °C), whereas warming in our simulations is prevailed by the synergy of soil mechanisms with feedbacks to vegetation, sea-ice and atmosphere (+0.24 °C), compared to our ASO-GCM simulations without soil scheme (HOL_CTL-PI_CTL: +0.10 °C). The change in solar forcing results in a warming of the high northern latitudes amplified through the interaction of the sea-ice albedo feedback (late autumn which continues into winter time), snow-vegetation feedback (winter period) and vegetation-soil feedback (throughout the year). Especially the start of snow-melt initiates earlier due to soils with lower albedo beneath which compensates for the effect of low spring insolation during mid-Holocene. Sundqvist et al. (2010a,b) reconstruct mid-Holocene climate north of 60° N by 2 °C warmer than Pre-industrial in annual mean, with seasonal variations of +1 °C in summer and +1.7 °C in winter. They conclude year round warming in the high northern latitudes is attributed to main warming during spring and/or autumn. Polar amplification > 60° N in our model study leads to +1.15 °C warming without – and to +1.83 °C

CPD
9, 2717–2770, 2013

with the soil scheme. Highest seasonal warming happens in winter (+2.37 °C) and autumn (+2.35 °C) consistent with increased solar radiation but not in agreement with +1 °C winter warming as stated by Sundqvist et al. (2010a,b). However, the multi-proxy approach might be biased due to an uneven clumping of proxy data in north Scandinavia and disproportionate high amount of terrestrial records compared to marine proxy archives (Sundqvist et al., 2010a,b; Otto et al., 2011). Nevertheless winter warming in high latitudes seems to be essential for northward migration of trees and expansion of temperate deciduous forests in Europe by reducing severity of coldest month temperature (Prentice et al., 2000). Otto et al. (2011) faced the problem of early spring warming by an atmosphere-vegetation model study, where they tested the climate sensitivity of increased snow masking by forest canopy. The atmosphere-vegetation feedback alone revealed a spring warming of 0.34 °C by an expansion in forest cover of 13 %, still not sufficient to explain the mismatch between model and proxy data (Otto et al., 2011). Although insolation during spring was reduced, HOL_sol warms about +0.98 °C, strongly pushed by the integrated soil feedback (+0.72 °C), which also contributes to warming through all seasons. Our model study simulates forest cover of +11 % in high (60–90° N) but does not show strong sensitivity of forest cover changes (+0.7 %) in mid-latitudes (35–60° N) as indicated by the pollen record (Prentice et al., 2000). Both Wohlfahrt et al. (2004) and Gallimore et al. (2005) find an increase in modelled grassland at mid-latitudes, once associated with spring warming (Wohlfahrt et al., 2004) and once with spring cooling (Gallimore et al., 2005). Mid-latitude anomalies of potential water storage capacities and wetness of soils show a moderate increase and spring temperatures are close to PI_sol (−0.07 °C), where lower spring insolation is compensated by the soil feedback (+0.4 °C). Though solar forcing is negative in spring, the soil and vegetation feedback (Wohlfahrt et al., 2004) potentially provide a mechanism for anomalous warming, closing the gap of model-data mismatch (Sundqvist et al., 2010a,b; Otto et al., 2011).

In Europe, an increased temperature anomaly, with warming in Scandinavia and cooling in Mediterranean region is suggested by the pollen record (Prentice et al., 2000;

CPD
9, 2717–2770, 2013

Bartlein et al., 2011). In consequence of mild winters in North Europe temperate deciduous forests expand in expense of boreal conifers (Prentice et al., 2000). Our model simulation shows mid-Holocene warming in North Europe amplified through changes in soil albedo in interaction with sea-ice retreat in the Barents Sea. However, the model simulation does not constitute an improvement compared to other simulations which fail to simulate cooling in the circum-Mediterranean region (Braconnot et al., 2007; Bartlein et al., 2011). A mid-Holocene cooling in the eastern Mediterranean region as e.g. seen in proxy data (Rimbu et al., 2003, and references therein), is captured in some models showing a tendency for a positive phase of AO/NAO during this time (Lorenz and Lohmann, 2004; Felis et al., 2004).

On the African continent the pollen data suggests an intrusion of xerophytic scrubs and northward shift of Savannah into Sahara ($\sim 20^{\circ}$ N, Prentice et al., 2000) enabled by increased precipitation (+200–500 mm yr^{-1}, Bartlein et al., 2011). Due to the Sahara desert soil parameterization pedogenesis does not happen further north than 20° N and 24° N latitude at the Arabian Peninsula, respectively. The strongest impact of simulated soils happens along a zonal band $\sim$ 13–17° N where precipitation increase $\sim$ 200–600 mm yr^{-1}, contributed by soils of $\sim$ 10–30 % and even $>$ 40 % at the Arabian Peninsula. However, this is still not sufficient to feed the catchment area of paleoloakes in south eastern Africa $\sim 20^{\circ}$ N (Vamborg et al., 2011; Hoelzmann et al., 2000). Apart from local water recycling and delayed water retention of soil processes the inclusion of wetlands and increased lake surface area might increase convective precipitation (Broström et al., 1998; Krinner et al., 2012). Further north the model climate simulation shows the evolution of grassland parallel to reduced desert appearance congruent to the records of Prentice et al. (2000).

The soil moisture feedback in monsoonal regions can be twofold. On one hand high soil moisture and thus large evaporation enhance precipitation and local water recycling. On the other hand, evaporative cooling reduces the land/ocean thermal gradient dampening moisture convergence over land. Douville et al. (2001), for instance, conducted soil moisture sensitivity studies in an AGCM for the Asian and African monsoon

CPD
9, 2717–2770, 2013

region. In their studies of locally increased soil moisture, the evaporative cooling effect dominated at the Indian continent resulting in a weaker monsoonal wind flow, whereas soil moisture positively feed back to precipitation in sub-Saharan Africa (Douville et al., 2001). As shown in the present work, mid-Holocene precipitation anomalies in typical monsoon areas are increased. In our approach, soil moisture and water holding field capacity of soils in these regions increase parallel with a darkening of soils which compensate for potential negative feedbacks of decreased moisture convergence.

In context of Holocene African wind system evolution, several mechanisms have been proposed for a zonal northward shift of the African rain belt and Indian monsoon (Wanner et al., 2008). Here, we can confirm that the soil feedback induce more forest cover and reduced desert appearance. As a consequence of the soil treatment, water holding field capacity and thus soil moisture increases in the Sahel zone reinforcing evaporation, precipitation and cloud cover. At 13° N latitude (and north India) lowered land albedo strengthens sensible heat flux in concurrence with increased soil water storage capacity leading to higher evapotranspiration, cloud cover and precipitation (soil moisture precipitation feedback) resulting in no significant surface temperature anomaly. Further north at 17° N latitude the darkening of land surface by soil albedo change dominates the anomalous warming in south Sahara resulting in an elevated latitudinal temperature gradient. In model simulations of the Eemian, Herold and Lohmann (2009) reveal a mechanism in which the latitudinal temperature difference above North Africa favors a stronger zonal pressure gradient. Along the gradient, zonal wind fields establish carrying Atlantic moisture inland. In agreement with simulations of the mid-Holocene (Braconnot et al., 2007), Herold and Lohmann (2009) conclude that this mechanism dominated during interglacials, where Earth's orbit favored increased seasonality and Northern Hemisphere insolation. In response to migration of vegetation soil development might have supported this mechanism, advecting more Atlantic moisture towards the African continent.

Kutzbach et al. (1996) prescribed effects of vegetation expansion, change in soil color and texture for mid-Holocene in an AGCM. Their results showed a strong positive

CPD
9, 2717–2770, 2013

feedback of soil characteristics reinforcing the monsoon, higher than changes in vegetation. Levis et al. (2004) utilized an AOGCM with dynamic vegetation and applied changes in soil albedo and soil texture. They concluded that West African monsoon is more sensitive to changes in land surface albedo rather than to changes of evapotranspiration. However, in their model approach a wettening of soils leads to halve of the respective albedo exhibiting a strong feedback in their model approach.

In a study using a vegetation module asynchronously coupled to a GCM, Gallimore et al. (2005) find a strong anomalous shift in forest cover increasing (+18 %) between 60–90° N and decreasing (−12 %) between 35–60° N. The expansion of grassland at the expense of forest mainly occurs in Eurasia which is affected by aridity (less precipitation and increased evapotranspiration) and lowered soil water content driven by enhanced summer solar radiation (Gallimore et al., 2005).

4.2 Dynamic soil feedback for the Last Glacial Maximum

The general picture of the model-data comparison fits for the glacial climate as it reflects year round cooling and continental drying with reduced precipitation (Bartlein et al., 2011). The soils reduce their ability to hold water against gravity accelerating their retention time and decreasing evaporation and the land surface appear brighter due to elevated soil albedo. In comparison to AOGCM modeling studies of PMIP2, the global cooling of surface air temperatures shown here (−7.03 °C MAT) exceed the cooling range of former studies (−3 to −6 °C, Braconnot et al., 2012; Braconnot et al., 2007) and cooling estimates based on proxy data (−4 °C; Annan and Hargreaves, 2013). As an example, modeled cooling in the tropical ocean is overestimated compared to the MARGO sea surface temperature compilation (MARGO Project members, 2009). However, PMIP2 studies do not take further negative radiative forcings into account (e.g. dust content; Jansen et al., 2007) which potentially amplify glacial cooling. Braconnot et al. (2012) associate part of the spread of cooling among the models with changes in surface albedo, for instance. In future climate scenarios, Hall et al. (2008) show that high values of prescribed snow albedo reduces the accumulation of snow during winter

CPD
9, 2717–2770, 2013

resulting in lower soil moistures in the subsequent summer, which reduces evaporation rates and hence latent heat transfer. Further, Otto et al. (2011) tested the sensitivity of modifying land surface albedo by varying the parameterized shading of forest canopy on snow. An increase of masking snow on the ground by forest canopy significantly increases spring warming (+0.34 °C north of 60° N latitude) in mid-Holocene simulations (Otto et al., 2011). Further, values of snow albedo in models of PMIP2 deviate and result in a differential magnitude of cooling clearly seen above prescribed LGM ice sheets (Braconnot et al., 2012). Braconnot et al. (2012) conclude that the insufficient representation of paleo monsoon in models questions the performance of present state of the art land surface schemes with dynamic vegetation integrated in AOGCMs in representing future land cover change. As the pedosphere is closely connected to terrestrial vegetation, e.g. plant available moisture, prescribed soil characteristics might impede vegetation to migrate across present-day climate zones.

The soil-feedback leads to further decreasing of precipitation, evaporation and surface temperatures in global mean. This leads to a broad expansion of desert areas in Eurasia, North Africa and north Polar Regions to the expense of grass cover. The expansion of polar desert in the Siberian sector in expense of C3-grasses leads to degradation and brightening of soils reinforcing cooling which shifts the northern tree line further southward more consistent with reconstructions (Prentice et al., 2000). In North America forests in close vicinity of the Laurentide ice sheet disappear in response to the regional cooling effect. Southeast North America exhibit an exceptional high precipitation anomaly caused by a southward deflection of the jet stream around the ice sheet which fosters tree growth there consistent with the terrestrial pollen record (Bartlein et al., 2011). In Europe basically models fail to reproduce extreme cooling of ∼ 20 °C in coldest month temperature which was reconstructed by pollen data (Braconnot et al., 2012; Bartlein et al., 2011). In west Europe the model produces a cooling of ∼ 18 °C with a sharp temperature gradient at the Mediterranean Sea declining towards Africa. The model with interactive soil scheme accounts for a surplus of cooling during the coldest month, which is in the range of global mean cooling due to the soil treatment

CPD
9, 2717–2770, 2013

(−1 °C). Kageyama et al. (2006) find an increased standard variation of coldest-month temperature in the PMIP2 models for Western Europe, up to three times higher than the control run. They argue that higher inter-annual variability of extreme cold events during the LGM might have biased the proxy record towards colder winter temperature reconstructions. Our model approach shows a similar increase of coldest-month temperature variability like in the PMIP2 models, only with minor changes due to the soil treatment. Most of the variability in our model as well as in the PMIP2 models is derived from changes in sea-ice cover in the North Atlantic impacting European climate (Kageyama et al., 2006).

In the tropics rainforests exhibit a strong contraction (−59 % in our simulation) caused by diminished evaporation, reduced water storage capacities in the atmosphere and hence less advective ocean to land moisture transport. Here the water holding field capacities and soil moisture are decreased, accelerating water retention time and impeding the uptake of plant available water in consequence. This is consistent with reconstructions of the rainforest, based on pollen, geochemical, and stable oxygen isotope data, indicating that Brazil rainforest decreased by 54 % and in Africa rainforest was decreased about 84 %, limited to viable conditions in the Congo basin (Anhuf et al., 2006).

In the Southern Hemisphere sea-ice expansion towards the equator leads to cooling and dry conditions as shown in the precipitation anomalies (Fig. 5). The latitudinal boundary at ∼ 45° S exhibit a transition of relative wet conditions in the north to Antarctic like paleoclimate conditions in the south as indicated by PMIP2 model simulations, which might have isolated the southern circumpolar region (Rojas et al., 2009). The general cooling in the tropical latitudes weakens the Hadley-cells and trade winds expressed by reduced convection, evaporation and precipitation in the ITCZ and less advective moisture transport by the weakened subtropical anticyclones. This results in an increased precipitation anomaly at the horse latitudes, with higher moisture transport towards land. The soil feedback leads to an additional cooling and weakening of the Hadley cells, as seen in positive precipitation anomalies caused by weakened

CPD
9, 2717–2770, 2013

South Indian, South Atlantic and South Pacific anticyclones. Evidence for colder and wetter conditions along the Southern Westerlies have been found in marine sediment cores close to the western margin of south-western Africa and subtropical South America (e.g. Stuut and Lamy, 2004) and ancient lake level stands in Bolivia (e.g. Baker et al., 2001). In general grain size distributions in both sediment cores of Stuut and Lamy (2004) reflect a declining trend of humidity from the last glacial towards Holocene in agreement with both of our time-slice experiments. The modeled vegetation responds to the positive glacial precipitation anomaly with higher occurrence of boreal forest. This is fostered by local water recycling associated with increased water storage capacities of soils in South Africa and South Australia. As a result the soil impact supports the development of boreal forests. Further the compilation of terrestrial pollen records of Bartlein et al. (2011) confirm increased plant available moisture for the South African region.

Jiang (2008) utilized an atmospheric GCM asynchronously coupled to the BIOME3 terrestrial vegetation equilibrium model and changed soil characteristics iteratively, similar to our approach. However, only if the dominant vegetation type in a grid cell has changed after iteration, soil characteristics were adapted as well. Instead we use the integrative mean of soil characteristics weighted on plant functional types per grid cell. Forced by LGM boundary conditions, the model of Jiang (2008) shows an additional decrease of surface air temperature of −0.05 °C globally, and high latitude (60–90° N) cooling over ice-free continental areas of −0.42 °C. The additional cooling trend presented in Jiang (2008) confirms, but however, it does not represent the magnitude of our findings. Some discrepancies might arise from differences in the setup of glacial boundary conditions (fixed SST fields as per CLIMAP, 1981; atmospheric CO_2 concentration of 200 ppmv versus 185 ppmv as used in our approach) or differences of prescribed soil characteristics attributed to vegetation types. Further, Jiang (2008) applies an atmospheric GCM which cannot consider potential ocean-atmosphere-sea interactions with terrestrial vegetation and soil.

CPD
9, 2717–2770, 2013

5 Conclusions

In this study, we develop a basic soil scheme which considers changes in physical soil characteristics with respect to computed canopy. Therefore changes of soil properties are tightly linked to vegetation dynamics and thus climate. Currently, some aspects of soil characteristics have been considered in GCMs, dynamically computed albedo of foliage for instance (Vamborg et al., 2011), but hitherto the integrated impact of soil formation with respect to soil albedo and water holding field capacities is untouched. The scheme is asynchronously coupled to an AOGCM with dynamical vegetation and tested for time slices of the Last Glacial Maximum and mid-Holocene. We show that the soil impact amplifies the climate signal for both, warmer and colder than pre-industrial simulations towards stronger extremes on a regional scale with global consequences.

The warm mid-Holocene climate is predominantly forced by a redistribution of solar radiation without changes in the total energy budget of incoming radiation, which claims for a strong feedback mechanism in the climate system. So far, most of the GCMs cannot reproduce the amplitude of warming as suggested by the geological remnants, raising the question of lacking or impeded feedbacks in present state of the art GCMs (O'ishi and Abe-Ouchi, 2011; Hargreaves et al., 2013; Lohmann et al., 2012). The soil feedback shown in the mid-Holocene simulation might serve as part of an explanation for these discrepancies.

In contrast the simulation with interactive soil treatment of the Last Glacial Maximum exhibits a global cooling beyond the range of the PMIP2 model simulations (Braconnot et al., 2007, 2012). On a regional scale the soil feedback improves the model performance getting closer to terrestrial proxies (increase in Sahara and polar desert area; decrease of tropical forests; extra cooling in north Siberia; increase in boreal forests along 30° S latitude; southward shift of the northern taiga/tundra transition; Anhuf et al., 2006; Prentice et al., 2000; Bartlein et al., 2011) or does not significantly contribute to a climate shift (e.g. Europe; Kageyama et al., 2006).

CPD
9, 2717–2770, 2013

So far we did not focus on vegetation and soil dynamics with respect to the global carbon budget. Apart from prescribed boundary conditions, the soil impact (e.g. water holding field capacity) might influence the uptake of CO_2 through coupled stomata transpiration by shifting the water stress regime. Further changes in water resources and soil temperature (through changes in soil albedo and water holding field capacities) might alter carbon sequestration and formation of soil carbon stocks, as happened throughout the last deglaciation (Adams et al., 1990; Brovkin et al., 2002; Ciais et al., 2011).

The nature of the soil scheme, similar to equilibrium terrestrial vegetation models (e.g. Prentice et al., 1992), does not account for soil evolution over time. Therefore it simulates a final solution of physical soil characteristics in equilibrium with vegetation and climate. For instance, the final state of the soil in the pre-industrial control run and mid-Holocene simulation leads to an anomalous warming, forest increase and desert decline in north eastern Canada, where the Laurentide ice-sheet retreat exposed juvenile soils during last deglaciation, starting carbon sequestration, which is still an ongoing process of present soil formation (Harden et al., 1992). However, time-slice experiments in general are designed to show an equilibrated climate state in the GCMs. Nevertheless future transient GCM studies utilizing dynamic soil schemes have to implement a time dependent function for nonlinear progressive and regressive soil development, acting on broad timescales (Johnson et al., 1990; Hoosbeek and Bryant, 1992). As shown in Claussen et al. (2006), only the fully integrated interaction of atmosphere, ocean and vegetation dynamics provided the strongest amplitude of climate variation by precessional forcing. In addition and analogy to vegetation dynamics (Claussen, 2009), we also show that the vegetation-soil feedback might reinforce the climate response to orbital forcing during the late Quaternary.

On tectonic timescales the model reproduction of a reduced meridional global temperature gradient with temperate climate in high latitudes has been identified as a key issue (e.g. Jenkyns et al., 2004; Moran et al., 2006; Huber and Caballero, 2011; Knorr et al., 2011; Krapp and Jungclaus, 2011; Salzmann et al., 2013). The introduction of

CPD
9, 2717–2770, 2013

dynamic soil feedbacks in climate models might be a pivotal aspect of climate sensitivity and potentially provides a solution for the equable climate enigma.

Acknowledgements. The authorship is grateful to Xu Zhang and Wei Wei for the model setup of Holocene and Last Glacial Maximum boundaries. The present work is supported through financial funding within the projects of the Deutsche Forschungsgemeinschaft, i.e. UCCC, PACES, REKLIM as well as the federal state Hessen (Germany) within the LOEWE initiative. Further we are thankful towards Johann Jungclaus and Victor Brovkin at Max Planck Institute for Meteorology in Hamburg (Germany) for providing the model code of COSMOS. We also wish to thank our colleague Arne Micheels for his collaboration.

References

Adams, J. M., Faure, H., Fauredenard, L., McGlade, J. M., and Woodward, F. I.: Increases in terrestrial carbon storage from the Last Glacial Maximum to the present, Nature, 348, 711–714, doi:10.1038/348711a0, 1990.

Anhuf, D., Ledru, M.-P., Behling, H., Da Cruz, F. W. J., Cordeiro, R. C., van der Hammen, T., Karmann, I., Marengo, J. A., d. Oliveira, P. E., Pessenda, L., Siffedine, A., Albuquerque, A. L., and Da Silva Dias, P. L.: Paleo-environmental change in Amazonian and African rainforest during the LGM, Palaeogeogr. Palaeocl., 239, 510–527, doi:10.1016/j.palaeo.2006.01.017, 2006.

Annan, J. D. and Hargreaves, J. C.: A new global reconstruction of temperature changes at the Last Glacial Maximum, Clim. Past, 9, 367–376, doi:10.5194/cp-9-367-2013, 2013.

Baker, P. A., Rigsby, C. A., Seltzer, G. O., Fritz, S. C., Lowenstein, T. K., Bacher, N. P., and Veliz, C.: Tropical climate changes at millennial and orbital timescales on the Bolivian Altiplano, Nature, 409, 698–701, doi:10.1038/35055524, 2001.

Bartlein, P. J., Harrison, S. P., Brewer, S., Connor, S., Davis, B. A. S., Gajewski, K., Guiot, J., Harrison-Prentice, T. I., Henderson, A., Peyron, O., Prentice, I. C., Scholze, M., Seppä, H., Shuman, B., Sugita, S., Thompson, R. S., Viau, A. E., Williams, J., and Wu, H.: Pollen-based continental climate reconstructions at 6 and 21 ka: a global synthesis, Clim. Dynam., 37, 775–802, doi:10.1007/s00382-010-0904-1, 2011.

Bergengren, J. C., Thompson, S. L., Pollard, D., and DeConto, R. M.: Modeling Global Climate–Vegetation Interactions in a Doubled CO_2 World, Climatic Change, 50, 31–75, doi:10.1023/A:1010609620103, 2001.

Berger, A. L.: Long-term variations of daily insolation and quaternary climatic changes, J. Atmos. Sci., 35, 2362–2367, doi:10.1175/1520-0469(1978)035<2362:LTVODI>2.0.CO;2, 1978.

Bonfils, C., de Noblet-Ducoudreé, N., Braconnot, P., and Joussaume, S.: Hot desert albedo and climate change: mid-Holocene monsoon in North Africa, J. Climate, 14, 3724–3737, doi:10.1175/1520-0442(2001)014<3724:HDAACC>2.0.CO;2, 2001.

Braconnot, P., Joussaume, S., Marti, O., and de Noblet, N.: Synergistic feedbacks from ocean and vegetation on the African monsoon response to mid-Holocene insolation, Geophys. Res. Lett., 26, 2481–2484, doi:10.1029/1999GL006047, 1999.

Braconnot, P., Otto-Bliesner, B., Harrison, S., Joussaume, S., Peterchmitt, J.-Y., Abe-Ouchi, A., Crucifix, M., Driesschaert, E., Fichefet, Th., Hewitt, C. D., Kageyama, M., Kitoh, A., Loutre, M.-F., Marti, O., Merkel, U., Ramstein, G., Valdes, P., Weber, L., Yu, Y., and Zhao, Y.: Results of PMIP2 coupled simulations of the Mid-Holocene and Last Glacial Maximum – Part 2: feedbacks with emphasis on the location of the ITCZ and mid- and high latitudes heat budget, Clim. Past, 3, 279–296, doi:10.5194/cp-3-279-2007, 2007.

Braconnot, P., Harrison, S. P., Kageyama, M., Bartlein, P. J., Masson-Delmotte, V., Abe-Ouchi, A., Otto-Bliesner, B., and Zhao, Y.: Evaluation of climate models using palaeoclimatic data, Nat. Clim. Change, 2, 417–424, doi:10.1038/NCLIMATE1456, 2012.

Broström, A., Coe, M., Harrison, S. P., Gallimore, R., Kutzbach, J. E., Foley, J., Prentice, I. C., and Behling, P.: Land surface feedbacks and palaeomonsoons in northern Africa, Geophys. Res. Lett., 25, 3615–3618, doi:10.1029/98GL02804, 1998.

Brovkin, V., Bendtsen, J., Claussen, M., Ganopolski, A., Kubatzki, C., Petoukhov, V., and Andreev, A.: Carbon cycle, vegetation, and climate dynamics in the Holocene: experiments with the CLIMBER-2 model, Global Biogeochem. Cy., 16, 1139, doi:10.1029/2001GB001662, 2002.

Brovkin, V., Raddatz, T., Reick, C. H., Claussen, M., and Gayler, V.: Global biogeophysical interactions between forest and climate, Geophys. Res. Lett., 36, L07405, doi:10.1029/2009GL037543, 2009.

CPD
9, 2717–2770, 2013

Carrington, D. P., Gallimore, R. G., and Kutzbach, J. E.: Climate sensitivity to wetlands and wetland vegetation in mid-Holocene North Africa, Clim. Dynam., 17, 151–157, doi:10.1007/s003820000099, 2001.

Charney, J., Quirk, W. J., Chow, S.-H., and Kornfield, J.: A comparative study of the effects of Albedo change on drought in semi–arid regions, J. Atmos. Sci., 34, 1366–1385, doi:10.1175/1520-0469(1977)034<1366:ACSOTE>2.0.CO;2, 1977.

Charney, J. G.: Dynamics of deserts and drought in the Sahel, Q. J. Roy. Meteorol. Soc., 101, 193–202, doi:10.1002/qj.49710142802, 1975.

Ciais, P., Tagliabue, A., Cuntz, M., Bopp, L., Scholze, M., Hoffmann, G., Lourantou, A., Harrison, S. P., Prentice, I. C., Kelley, D. I., Koven, C., and Piao, S. L.: Large inert carbon pool in the terrestrial biosphere during the Last Glacial Maximum, Nat. Geosci., 5, 74–79, doi:10.1038/NGEO1324, 2012.

Claussen, M.: On coupling global biome models with climate models, Clim. Res., 4, 203–221, 1994.

Claussen, M.: Modeling bio-geophysical feedback in the African and Indian monsoon region, Clim. Dynam., 13, 247–257, doi:10.1007/s003820050164, 1997.

Claussen, M.: Late Quaternary vegetation-climate feedbacks, Clim. Past, 5, 203–216, doi:10.5194/cp-5-203-2009, 2009.

Claussen, M. and Gayler, V.: The greening of the Sahara during the mid-Holocene: results of an interactive atmosphere-biome model, Global Ecol. Biogeogr., 6, 369–377, doi:10.2307/2997337, 1997.

Claussen, M., Fohlmeister, J., Ganopolski, A., and Brovkin, V.: Vegetation dynamics amplifies precessional forcing, Geophys. Res. Lett., 33, L09709, doi:10.1029/2006GL026111, 2006.

CLIMAP: Seasonal Reconstruction of the Earth's Surface at the Last Glacial Maximum, Geological Society of America Map and Chart Series MC-36, Geological Society of America, Boulder, Colorado, 1981.

Coe, M. T. and Bonan, G. B.: Feedbacks between climate and surface water in northern Africa during the middle Holocene, J. Geophys. Res.-Atmos., 102, 11087–11101, doi:10.1029/97JD00343, 1997.

deMenocal, P. B. and Rind, D.: Sensitivity of Asian and African climate to variations in seasonal insolation, glacial ice cover, sea surface temperature, and Asian orography, J. Geophys. Res.-Atmos., 98, 7265–7287, doi:10.1029/92JD02924, 1993.

CPD
9, 2717–2770, 2013

Doherty, R., Kutzbach, J., Foley, J., and Pollard, D.: Fully coupled climate/dynamical vegetation model simulations over Northern Africa during the mid-Holocene, Clim. Dynam., 16, 561–573, doi:10.1007/s003820000065, 2000.

Douville, H., Chauvin, F., and Broqua, H.: Influence of soil moisture on the Asian and African monsoons, Part I: mean monsoon and daily precipitation, J. Climate, 14, 2381–2403, doi:10.1175/1520-0442(2001)014<2381:IOSMOT>2.0.CO;2, 2001.

Douville, H., Conil, S., Tyteca, S., and Voldoire, A.: Soil moisture memory and West African monsoon predictability: artefact or reality?, Clim. Dynam., 28, 723–742, doi:10.1007/s00382-006-0207-8, 2007.

Dupont, L.: Orbital scale vegetation change in Africa, Quaternary Sci. Rev., 30, 3589–3602, doi:10.1016/j.quascirev.2011.09.019, 2011.

Felis, T., Lohmann, G., Kuhnert, H., Lorenz, S. J., Scholz, D., Pätzold, J., Al-Rousan, S. A., and Al-Moghrabi, S. M.: Increased seasonality in Middle East temperatures during the last interglacial period, Nature, 429, 164–168, doi:10.1038/nature02546, 2004.

Foley, J. A., Kutzbach, J. E., Coe, M. T., and Levis, S.: Feedbacks between climate and boreal forests during the Holocene epoch, Nature, 371, 52–54, doi:10.1038/371052a0, 1994.

Foley, J. A., Levis, S., Costa, M. H., Cramer, W., and Pollard, D.: Incorporating dynamic vegetation cover within global climate models, Ecol. Appl., 10, 1620–1632, doi:10.2307/2641227, 2000.

Foley, J. A., Coe, M. T., Scheffer, M., and Wang, G.: Regime shifts in the Sahara and Sahel: interactions between ecological and climatic systems in Northern Africa, Ecosystems, 6, 524–532, doi:10.1007/s10021-002-0227-0, 2003.

Gallimore, R., Jacob, R., and Kutzbach, J.: Coupled atmosphere-ocean-vegetation simulations for modern and mid-Holocene climates: role of extratropical vegetation cover feedbacks, Clim. Dynam., 25, 755–776, doi:10.1007/s00382-005-0054-z, 2005.

Gong, X., Knorr, G., Lohmann, G., and Zhang, X.: Dependence of abrupt Atlantic meridional ocean circulation changes on climate background states, Geophys. Res. Lett., in revision, 2013.

Hagemann, S.: An Improved Land Surface Parameter Dataset for Global and Regional Climate Models, Rep. 336, Max-Planck-Institut für Meteorologie, Hamburg, 2002.

Hagemann, S., Botzet, M., Dümenil, L., and Machenhauer, B.: Derivation of Global GCM Boundary Conditions from 1 km Land Use Satellite Data, Rep. 289, Max-Planck-Institut für Meteorologie, Hamburg, 1999.

CPD
9, 2717–2770, 2013

Hall, A., Qu, X., and Neelin, J. D.: Improving predictions of summer climate change in the United States, Geophys. Res. Lett., 35, L01702, doi:10.1029/2007GL032012, 2008.
Harden, J. W., Sundquist, E. T., Stallard, R. F., and Mark, R. K.: Dynamics of soil carbon during deglaciation of the Laurentide ice-sheet, Science, 258, 1921–1924, doi:10.1126/science.258.5090.1921, 1992.
Hargreaves, J. C., Annan, J. D., Ohgaito, R., Paul, A., and Abe-Ouchi, A.: Skill and reliability of climate model ensembles at the Last Glacial Maximum and mid-Holocene, Clim. Past, 9, 811–823, doi:10.5194/cp-9-811-2013, 2013.
Henderson-Sellers, A.: Continental vegetation as a dynamic component of a global climate model: a preliminary assessment, Climatic Change, 23, 337–377, doi:10.1007/BF01091622, 1993.
Henderson-Sellers, A., Wilson, M. F., Thomas, G., and Dickinson, R. E.: Current Global Land-Surface Data Sets for Use in Climate-Related Studies, NCAR Technical Note 272, Boulder, Colorado, 1986.
Herold, M. and Lohmann, G.: Eemian tropical and subtropical African moisture transport: an isotope modelling study, Clim. Dynam., 33, 1075–1088, doi:10.1007/s00382-008-0515-2, 2009.
Hoelzmann, P., Jolly, D., Harrison, S. P., Laarif, F., Bonnefille, R., and Pachur, H.-J.: Mid-Holocene land-surface conditions in northern Africa and the Arabian Peninsula: a data set for the analysis of biogeophysical feedbacks in the climate system, Global Biogeochem. Cy., 12, 35–51, doi:10.1029/97GB02733, 1998.
Hoelzmann, P., Kruse, H.-J., and Rottinger, F.: Precipitation estimates for the eastern Saharan palaeomonsoon based on a water balance model of the West Nubian Palaeolake Basin, Paleomonsoon variations and terrestrial environmental change, Global Planet. Change, 26, 105–120, doi:10.1016/S0921-8181(00)00038-2, 2000.
Holdridge, L. R.: Determination of world plant formations from simple climatic data, Science, 105, 367–368, doi:10.1126/science.105.2727.367, 1947.
Hoosbeek, M. R. and Bryant, R. B.: Towards the quantitative modeling of pedogenesis – a review, Geoderma, 55, 183–210, doi:10.1016/0016-7061(92)90083-J, 1992.
Huber, M. and Caballero, R.: The early Eocene equable climate problem revisited, Clim. Past, 7, 603–633, doi:10.5194/cp-7-603-2011, 2011.
Jansen, E., Overpeck, J., Briffa, K., Duplessy, J.-C., Joos, F., Masson-Delmotte, V., Olago, D., Otto-Bliesner, B., Peltier, W., Rahmstorf, S., Ramesh, R., Raynaud, D., Rind, D.,

CPD
9, 2717–2770, 2013

Solomina, O., Villalba, R., and Zhang, D.: Palaeoclimate, in: Climate Change 2007: The Physical Science Basis, Contribution of Working Group I to the Fourth Assessment Report of the Intergovernmental Panel on Climate Change, chap, Palaeoclimate, Cambridge University Press, Cambridge, UK and New York, NY, USA, 2007.

Jenkyns, H., Forster, A., Schouten, S., and Damste, J.: High temperatures in the Late Cretaceous Arctic Ocean, Nature, 432, 888–892, doi:10.1038/nature03143, 2004.

Jenny, H.: Factors of Soil Formation, McGraw-Hill Book Company, New York, London, 1941.

Jiang, D.: Vegetation and soil feedbacks at the Last Glacial Maximum, Palaeogeogr. Palaeocl., 268, 39–46, doi:10.1016/j.palaeo.2008.07.023, 2008.

Johnson, D. L., Keller, E. A., and Rockwell, T. K.: Dynamic pedogenesis: new views on some key soil concepts, and a model for interpreting quaternary soils, Quaternary Res., 33, 306–319, doi:10.1016/0033-5894(90)90058-S, 1990.

Jungclaus, J. H., Keenlyside, N., Botzet, M., Haak, H., Luo, J.-J., Latif, M., Marotzke, J., Mikolajewicz, U., and Roeckner, E.: Ocean circulation and tropical variability in the coupled model ECHAM5/MPI-OM, J. Climate, 19, 3952–3972, 2006.

Kageyama, M., Laîné, A., Abe-Ouchi, A., Braconnot, P., Cortijo, E., Crucifix, M., Vernal, A. D., Guiot, J., Hewitt, C. D., Kitoh, A., Kucera, M., Marti, O., Ohgaito, R., Otto-Bliesner, B., Peltier, W. R., Rosell-Melé, A., Vettoretti, G., Weber, S. L., and Yu, Y.: Last Glacial Maximum temperatures over the North Atlantic, Europe and western Siberia: a comparison between PMIP models, MARGO sea-surface temperatures and pollen-based reconstructions, Quaternary Sci. Rev., 25, 2082–2102, doi:10.1016/j.quascirev.2006.02.010, 2006.

Knorr, G., Butzin, M., Micheels, A., and Lohmann, G.: A warm Miocene climate at low atmospheric CO_2 levels, Geophys. Res. Lett., 38, L20701, doi:10.1029/2011GL048873, 2011.

Knorr, W.: Annual and interannual CO_2 exchanges of the terrestrial biosphere: process-based simulations and uncertainties, Global Ecol. Biogeogr., 9, 225–252, doi:10.1046/j.1365-2699.2000.00159.x, 2000.

Knorr, W. and Schnitzler, K. G.: Enhanced albedo feedback in North Africa from possible combined vegetation and soil-formation processes, Clim. Dynam., 26, 55–63, doi:10.1007/s00382-005-0073-9, 2006.

Krapp, M. and Jungclaus, J. H.: The Middle Miocene climate as modelled in an atmosphere-ocean-biosphere model, Clim. Past, 7, 1169–1188, doi:10.5194/cp-7-1169-2011, 2011.

CPD
9, 2717–2770, 2013

Krinner, G., Lezine, A. M., Braconnot, P., Sepulchre, P., Ramstein, G., Grenier, C., and Gouttevin, I.: A reassessment of lake and wetland feedbacks on the North African Holocene climate, Geophys. Res. Lett., 39, L07701, doi:10.1029/2012GL050992, 2012.

Kump, L. R. and Pollard, D.: Amplification of Cretaceous warmth by biological cloud feedbacks, Science, 320, 195, doi:10.1126/science.1153883, 2008.

Kutzbach, J. E. and Guetter, P. J.: The influence of changing orbital parameters and surface boundary conditions on climate simulations for the past 18 000 years, J. Atmos. Sci., 43, 1726–1759, 1986.

Kutzbach, J. E. and Liu, Z.: Response of the African Monsoon to orbital forcing and ocean feedbacks in the middle Holocene, Science, 278, 440–443, doi:10.1126/science.278.5337.440, 1997.

Kutzbach, J. E. and Otto-Bliesner, B. L.: The sensitivity of the African-Asian monsoonal climate to orbital parameter changes for 9000 years BP in a low-resolution general circulation model, J. Atmos. Sci., 39, 1177–1188, 1982.

Kutzbach, J. E. and Street-Perrott, F. A.: Milankovitch forcing of fluctuations in the level of tropical lakes from 18 to 0 kyr BP, Nature, 317, 130–134, doi:10.1038/317130a0, 1985.

Kutzbach, J. E., Bonan, G., Foley, J., and Harrison, S. P.: Vegetation and soil feedbacks on the response of the African monsoon to orbital forcing in the early to middle Holocene, Nature, 384, 623–626, doi:10.1038/384623a0, 1996.

Levis, S., Bonan, G. B., and Bonfils, C.: Soil feedback drives the mid-Holocene North African monsoon northward in fully coupled CCSM2 simulations with a dynamic vegetation model, Clim. Dynam., 23, 791–802, doi:10.1007/s00382-004-0477-y, 2004.

Lohmann, G., Pfeiffer, M., Laepple, T., Leduc, G., and Kim, J.-H.: A model-data comparison of the Holocene global sea surface temperature evolution, Clim. Past Discuss., 8, 1005–1056, doi:10.5194/cpd-8-1005-2012, 2012.

Lorenz, S. and Lohmann, G.: Acceleration technique for Milankovitch type forcing in a coupled atmosphere-ocean circulation model: method and application for the Holocene, Clim. Dynam., 23, 727–743, doi:10.1007/s00382-004-0469-y, 2004.

Lunt, D. J., Abe-Ouchi, A., Bakker, P., Berger, A., Braconnot, P., Charbit, S., Fischer, N., Herold, N., Jungclaus, J. H., Khon, V. C., Krebs-Kanzow, U., Langebroek, P. M., Lohmann, G., Nisancioglu, K. H., Otto-Bliesner, B. L., Park, W., Pfeiffer, M., Phipps, S. J., Prange, M., Rachmayani, R., Renssen, H., Rosenbloom, N., Schneider, B., Stone, E. J., Takahashi, K.,

CPD
9, 2717–2770, 2013

Wei, W., Yin, Q., and Zhang, Z. S.: A multi-model assessment of last interglacial temperatures, Clim. Past, 9, 699–717, doi:10.5194/cp-9-699-2013, 2013.
Marsland, S. J., Haak, H., Jungclaus, J. H., Latif, M., and Röske, F.: The Max-Planck-Institute global ocean/sea ice model with orthogonal curvilinear coordinates, Ocean Modell., 5, 91–127, doi:10.1016/S1463-5003(02)00015-X, 2003.
McIntosh, S. K. and McIntosh, R. J.: Current directions in West-African prehistory, Annu. Rev. Anthropol., 12, 215–258, doi:10.1146/annurev.an.12.100183.001243, 1983.
Meinshausen, M., Smith, S. J., Calvin, K., Daniel, J. S., Kainuma, M. L. T., Lamarque, J.-F., Matsumoto, K., Montzka, S. A., Raper, S. C. B., Riahi, K., Thomson, A., Velders, G. J. M., and Vuuren, D. P. P.: The RCP greenhouse gas concentrations and their extensions from 1765 to 2300, Climatic Change, 109, 213–241, doi:10.1007/s10584-011-0156-z, 2011.
Micheels, A., Eronen, J., and Mosbrugger, V.: The late Miocene climate response to a modern Sahara desert, Global Planet. Change, 67, 193–204, doi:10.1016/j.gloplacha.2009.02.005, 2009.
Moran, K., Backman, J., Brinkhuis, H., Clemens, S. C., Cronin, T., Dickens, G. R., Eynaud, F., Gattacceca, J., Jakobsson, M., Jordan, R. W., Kaminski, M., King, J., Koc, N., Krylov, A., Martinez, N., Matthiessen, J., McInroy, D., Moore, T. C., Onodera, J., O'Regan, M., Palike, H., Rea, B., Rio, D., Sakamoto, T., Smith, D. C., Stein, R., St John, K., Suto, I., Suzuki, N., Takahashi, K., Watanabe, M., Yamamoto, M., Farrell, J., Frank, M., Kubik, P., Jokat, W., and Kristoffersen, Y.: The Cenozoic palaeoenvironment of the Arctic Ocean, Nature, 441, 601–605, doi:10.1038/nature04800, 2006.
Nicholson, S. E., Tucker, C. J., and Ba, M. B.: Desertification, Drought, and Surface Vegetation: An Example from the West African Sahel, B. Am. Meteorol. Soc., 79, 815–829, doi:10.1175/1520-0477(1998)079<0815:DDASVA>2.0.CO;2, 1998.
O'ishi, R. and Abe-Ouchi, A.: Polar amplification in the mid-Holocene derived from dynamical vegetation change with a GCM, Geophys. Res. Lett., 38, L14702, doi:10.1029/2011GL048001, 2011.
Otto, J., Raddatz, T., and Claussen, M.: Climate variability-induced uncertainty in mid-Holocene atmosphere–ocean–vegetation feedbacks, Geophys. Res. Lett., 36, L23710, doi:10.1029/2009GL041457, 2009a.
Otto, J., Raddatz, T., Claussen, M., Brovkin, V., and Gayler, V.: Separation of atmosphere–ocean–vegetation feedbacks and synergies for mid-Holocene climate, Geophys. Res. Lett., 36, L09701, doi:10.1029/2009GL037482, 2009b.

CPD
9, 2717–2770, 2013

Otto, J., Raddatz, T., and Claussen, M.: Strength of forest-albedo feedback in mid-Holocene climate simulations, Clim. Past, 7, 1027–1039, doi:10.5194/cp-7-1027-2011, 2011.
Otto-Bliesner, B. L. and Upchurch, G. R.: Vegetation-induced warming of high-latitude regions during the Late Cretaceous period, Nature, 385, 804–807, doi:10.1038/385804a0, 1997.
Pagani, M., Liu, Z., LaRiviere, J., and Ravelo, A. C.: High Earth-system climate sensitivity determined from Pliocene carbon dioxide concentrations, Nat. Geosci., 3, 27–30, doi:10.1038/NGEO724, 2010.
Petit, J.-R., Jouzel, J., Raynaud, D., Barkov, N., Barnola, J.-M., Basile, I., Bender, M., Chappellaz, J., Davis, M., Delaygue, G., Delmotte, M., Kotlyakov, V. M., Legrand, M., Lipenkov, V. Y., Lorius, C., Pepin, L., Ritz, C., Saltzman, E., and Stievenard, M.: Climate and atmospheric history of the past 420 000 years from the Vostok ice core, Antarctica, Nature, 399, 429–436, 1999.
Petit-Maire, N.: Interglacial environments in presently hyperarid Sahara: palaeoclimatic implications, in: Paleoclimatology and Paleometeorology: Modern and Past Patterns of Global Atmospheric Transport, edited by: Leinen, M. and Sarnthein, M., vol. 282 of NATO ASI Series, Springer Netherlands, 637–661, 1989.
Petit-Maire, N. and Riser, J.: Holocene lake deposits and palaeoenvironments in Central Sahara, northeastern Mali, Palaeogeogr. Palaeocl., 35, 45–61, doi:10.1016/0031-0182(81)90093-6, 1981.
Prentice, I. C., Cramer, W., Harrison, S. P., Leemans, R., Monserud, R. A., and Solomon, A. M.: Special paper: a global biome model based on plant physiology and dominance, soil properties and climate, J. Biogeogr., 19, 117–134, doi:10.2307/2845499, 1992.
Prentice, I. C., Jolly, D., and BIOME 6000 participants: Mid-Holocene and glacial maximum vegetation geography of the northern continents and Africa, J. Biogeogr., 27, 507–519, doi:10.1046/j.1365-2699.2000.00425.x, 2000.
Raddatz, T. J., Reick, C. H., Knorr, W., Kattge, J., Roeckner, E., Schnur, R., Schnitzler, K.-G., Wetzel, P., and Jungclaus, J.: Will the tropical land biosphere dominate the climate–carbon cycle feedback during the twenty-first century?, Clim. Dynam., 29, 565–574, 2007.
Rechid, D., Raddatz, T. J., and Jacob, D.: Parameterization of snow-free land surface albedo as a function of vegetation phenology based on MODIS data and applied in climate modelling, Theor. Appl. Climatol., 95, 245–255, doi:10.1007/s00704-008-0003-y, 2009.

CPD
9, 2717–2770, 2013

Rimbu, N., Lohmann, G., Kim, J.-H., Arz, H. W., and Schneider, R.: Arctic/North Atlantic Oscillation signature in Holocene sea surface temperature trends as obtained from alkenone data, Geophys. Res. Lett., 30, 1280, doi:10.1029/2002GL016570, 2003.

Roeckner, E., Arpe, K., Bengtsson, L., Brinkop, S., Dümenil, L., Esch, M., Kirk, E., Lunkeit, F., Ponater, M., Rockel, B., Sausen, R., Schlese, U., Schubert, S., and Windelband, M. (Eds.): Simulation of the Present-Day Climate with ECHAM Model: Impact of Model Physics and Resolution, Report 93, Max-Planck-Institut für Meteorologie, Hamburg, 1992.

Roeckner, E., Bäuml, G., Bonaventura, L., Brokopf, R., Esch, M., Giorgetta, M., Hagemann, S., Kirchner, I., Kornblueh, L., Manzini, E., Rhodin, A., Schlese, U., Schulzweida, U., and Tompkins, A.: The Atmospheric General Circulation Model ECHAM5, Part I: Model Description, Rep. 349, Max-Planck-Institut für Meteorologie, Hamburg, 2003.

Roeckner, E., Brokopf, R., Esch, M., Giorgetta, M., Hagemann, S., Kornblueh, L., Manzini, E., Schlese, U., and Schulzweida, U.: Sensitivity of simulated climate to horizontal and vertical resolution in the ECHAM5 atmosphere model, J. Climate, 19, 3771–3791, 2006.

Rojas, M., Moreno, P., Kageyama, M., Crucifix, M., Hewitt, C., Abe-Ouchi, A., Ohgaito, R., Brady, E. C., and Hope, P.: The southern Westerlies during the last glacial maximum in PMIP2 simulations, Clim. Dynam., 32, 525–548, doi:10.1007/s00382-008-0421-7, 2009.

Salzmann, U., Dolan, A., Haywood, A., Chan, W.-L., Hill, D., Abe-Ouchi, A., Otto-Bliesner, B., Bragg, F., Chandler, M., Contoux, C., Jost, A., Kamae, Y., Lohmann, G., Lunt, D., Pickering, S., Pound, M., Ramstein, G., Rosenbloom, N., Sohl, L., Stepanek, C., Ueda, H., and Zhang, Z.: How well do models reproduce warm terrestrial climates of the Pliocene?, Nat. Clim. Change, in revision, 2013.

Schurgers, G., Mikolajewicz, U., Groeger, M., Maier-Reimer, E., Vizcaino, M., and Winguth, A.: The effect of land surface changes on Eemian climate, Clim. Dynam., 29, 357–373, doi:10.1007/s00382-007-0237-x, 2007.

Seneviratne, S. I., Koster, R. D., Guo, Z., Dirmeyer, P. A., Kowalczyk, E., Lawrence, D., Liu, P., Mocko, D., Lu, C.-H., Oleson, K. W., and Verseghy, D.: Soil moisture memory in AGCM simulations: analysis of Global Land–Atmosphere Coupling Experiment (GLACE) data, J. Hydrometeorol., 7, 1090–1112, doi:10.1175/JHM533.1, 2006.

Seneviratne, S. I., Corti, T., Davin, E. L., Hirschi, M., Jaeger, E. B., Lehner, I., Orlowsky, B., and Teuling, A. J.: Investigating soil moisture–climate interactions in a changing climate: a review, Earth-Sci. Rev., 99, 125–161, doi:10.1016/j.earscirev.2010.02.004, 2010.

CPD
9, 2717–2770, 2013

Shellito, C. J. and Sloan, L. C.: Reconstructing a lost Eocene Paradise, Part II: on the utility of dynamic global vegetation models in pre-quaternary climate studies, Global Planet. Change, 50, 18–32, doi:10.1016/j.gloplacha.2005.08.002, 2006.
Sloan, L. C. and Morrill, C.: Orbital forcing and Eocene continental temperatures, Palaeogeogr. Palaeocl., 144, 21–35, doi:10.1016/S0031-0182(98)00091-1, 1998.
Sloan, L. C. and Pollard, D.: Polar stratospheric clouds: a high latitude warming mechanism in an ancient greenhouse world, Geophys. Res. Lett., 25, 3517–3520, doi:10.1029/98GL02492, 1998.
Sloan, L. C., Walker, J. C. G., and Moore, T. C.: Possible role of oceanic heat transport in Early Eocene climate, Paleoceanography, 10, 347–356, doi:10.1029/94PA02928, 1995.
Stein, U. and Alpert, P.: Factor separation in numerical simulations, J. Atmos. Sci., 50, 2107–2115, doi:10.1175/1520-0469(1993)050<2107:FSINS>2.0.CO;2, 1993.
Stepanek, C. and Lohmann, G.: Modelling mid-Pliocene climate with COSMOS, Geosci. Model Dev., 5, 1221–1243, doi:10.5194/gmd-5-1221-2012, 2012.
Stuut, J.-B. W. and Lamy, F.: Climate variability at the southern boundaries of the Namib (southwestern Africa) and Atacama (northern Chile) coastal deserts during the last 120 000 yr, Quaternary Res., 62, 301–309, doi:10.1016/j.yqres.2004.08.001, 2004.
Sundqvist, H. S., Zhang, Q., Moberg, A., Holmgren, K., Körnich, H., Nilsson, J., and Brattström, G.: Climate change between the mid and late Holocene in northern high latitudes – Part 1: Survey of temperature and precipitation proxy data, Clim. Past, 6, 591–608, doi:10.5194/cp-6-591-2010, 2010a.
Sundqvist, H. S., Zhang, Q., Moberg, A., Holmgren, K., Körnich, H., Nilsson, J., and Brattström, G.: Corrigendum to "Climate change between the mid and late Holocene in northern high latitudes – Part 1: Survey of temperature and precipitation proxy data" published in Clim. Past, 6, 591–608, 2010, Clim. Past, 6, 739–743, doi:10.5194/cp-6-739-2010, 2010b.
Texier, D., de Noblet, N., Harrison, S. P., Haxeltine, A., Jolly, D., Joussaume, S., Laarif, F., Prentice, I. C., and Tarasov, P.: Quantifying the role of biosphere-atmosphere feedbacks in climate change: coupled model simulations for 6000 years BP and comparison with palaeodata for northern Eurasia and northern Africa, Clim. Dynam., 13, 865–882, doi:10.1007/s003820050202, 1997.
Texier, D., de Noblet, N., and Braconnot, P.: Sensitivity of the African and Asian monsoons to mid-Holocene insolation and data-inferred surface changes, J. Climate, 13, 164–181, doi:10.1175/1520-0442(2000)013<0164:SOTAAA>2.0.CO;2, 2000.

CPD
9, 2717–2770, 2013

Valdes, P.: Built for stability, Nat. Geosci., 4, 414–416, 2011.
Vamborg, F. S. E., Brovkin, V., and Claussen, M.: The effect of a dynamic background albedo scheme on Sahel/Sahara precipitation during the mid-Holocene, Clim. Past, 7, 117–131, doi:10.5194/cp-7-117-2011, 2011.
Varma, V., Prange, M., Merkel, U., Kleinen, T., Lohmann, G., Pfeiffer, M., Renssen, H., Wagner, A., Wagner, S., and Schulz, M.: Holocene evolution of the Southern Hemisphere westerly winds in transient simulations with global climate models, Clim. Past, 8, 391–402, doi:10.5194/cp-8-391-2012, 2012.
Waelbroeck, C., Paul, A., Kucera, M., Rosell-Mele, A., Weinelt, M., Schneider, R., Mix, A. C., Abelmann, A., Armand, L., Bard, E., Barker, S., Barrows, T. T., Benway, H., Cacho, I., Chen, M. T., Cortijo, E., Crosta, X., de Vernal, A., Dokken, T., Duprat, J., Elderfield, H., Eynaud, F., Gersonde, R., Hayes, A., Henry, M., Hillaire-Marcel, C., Huang, C. C., Jansen, E., Juggins, S., Kallel, N., Kiefer, T., Kienast, M., Labeyrie, L., Leclaire, H., Londeix, L., Mangin, S., Matthiessen, J., Marret, F., Meland, M., Morey, A. E., Mulitza, S., Pflaumann, U., Pisias, N. G., Radi, T., Rochon, A., Rohling, E. J., Sbaffi, L., Schaefer-Neth, C., Solignac, S., Spero, H., Tachikawa, K., Turon, J. L., and Members, M. P.: Constraints on the magnitude and patterns of ocean cooling at the Last Glacial Maximum, Nat. Geosci., 2, 127–132, doi:10.1038/NGEO411, 2009.
Wang, H. J.: Role of vegetation and soil in the Holocene megathermal climate over China, J. Geophys. Res.-Atmos., 104, 9361–9367, doi:10.1029/1999JD900049, 1999.
Wanner, H., Beer, J., Bütikofer, J., Crowley, T. J., Cubasch, U., Flückiger, J., Goosse, H., Grosjean, M., Joos, F., Kaplan, J. O., Küttel, M., Müller, S. A., Prentice, I. C., Solomina, O., Stocker, T. F., Tarasov, P., Wagner, M., and Widmann, M.: Mid- to Late Holocene climate change: an overview, Quaternary Sci. Rev., 27, 1791–1828, doi:10.1016/j.quascirev.2008.06.013, 2008.
Wei, W. and Lohmann, G.: Simulated Atlantic Multidecadal Oscillation during the Holocene, J. Climate, 25, 6989–7002, doi:10.1175/JCLI-D-11-00667.1, 2012.
Wei, W., Lohmann, G., and Dima, M.: Distinct modes of internal variability in the global meridional overturning circulation associated with the Southern Hemisphere westerly winds, J. Phys. Oceanogr., 42, 785–801, doi:10.1175/JPO-D-11-038.1, 2012.
Willeit, M., Ganopolski, A., and Feulner, G.: On the effect of orbital forcing on mid-Pliocene climate, vegetation and ice sheets, Clim. Past Discuss., 9, 1703–1734, doi:10.5194/cpd-9-1703-2013, 2013.

CPD
9, 2717–2770, 2013

Williamson, D. L., Kiehl, J. T., Ramanathan, V., Dickinson, R. E., and Hack, J. J.: Description of NCAR community climate model (CCM1), Climate and Global Dynamics Division, National Center for Atmospheric Research, Boulder, Colorado, 1987.

Wohlfahrt, J., Harrison, S. P., and Braconnot, P.: Synergistic feedbacks between ocean and vegetation on mid- and high-latitude climates during the mid-Holocene, Clim. Dynam., 22, 223–238, doi:10.1007/s00382-003-0379-4, 2004.

Zhang, X., Lohmann, G., Knorr, G., and Xu, X.: Two ocean states during the Last Glacial Maximum, Clim. Past Discuss., 8, 3015–3041, doi:10.5194/cpd-8-3015-2012, 2012.

Zhao, Y., Braconnot, P., Marti, O., Harrison, S. P., Hewitt, C., Kitoh, A., Liu, Z., Mikolajewicz, U., Otto-Bliesner, B., and Weber, S. L.: A multi-model analysis of the role of the ocean on the African and Indian monsoon during the mid-Holocene, Clim. Dynam., 25, 777–800, doi:10.1007/s00382-005-0075-7, 2005.

CPD
9, 2717–2770, 2013

Table 1. Physical characteristics of soil tiles.

Soil tiles based on calculated PFTs	h_{cws} (total water holding field capacity of soil) (m)	soil texture (FAO soil data flags)	α_{vis}, soil albedo VIS (0.3–0.7 µm)	α_{nir}, soil albedo NIR (0.7–3 µm)
tropical broadleaved evergreen forest	0.77	loam and clay	0.12	0.20
tropical deciduous broadleaved forest	0.73	loam	0.18	0.34
temper./boreal evergreen forest	0.50	loam	0.08	0.10
temper./boreal deciduous forest	0.58	loam	0.09	0.11
raingreen shrubs	0.68	loam	0.12	0.17
C3 perennial grass				
C3 perennial grass > 0 °C MAT	0.77	loam	0.12	0.21
C3 perennial grass/cold shrubs (tundra) < 0 °C MAT	0.23	loam	0.08	0.13
C4 perennial grass	1.07	loam	0.14	0.26
desert fraction				
desert fraction global	0.17	loam	0.20	0.37
desert fraction in Sahara, Arabian Peninsula > 50 % (13–35.26° N)	0.11	loam	0.25	0.49

CPD
9, 2717–2770, 2013

Table 2. Global anomalies of land surface characteristics and the contribution of soil feedback for mid-Holocene and Last Glacial Maximum model studies.

	HOL_sol-CTL_sol (syn)	LGM_sol-CTL_sol (syn)	LGM_sol-CTL_sol without exposed shelves (syn)
soil wetness (cm)	1.85 (+1.26)	3.03 (−4.5)	−3.66 (−5.69)
snow depth (in mm water equivalent)	−0.21 (−0.36)	31.6 (−39.3)	9.08 (+8.28)
snow fall ($kg\,m^{-2}\,yr^{-1}$)	−1.03 (−1.25)	−16.9 (+4.26)	16.37 (+3.85)
surface runoff and drainage ($kg\,m^{-2}\,yr^{-1}$)	6.72 (+3.35)	−23.8 (+2.62)	−4.89 (+3.69)
land evaporation ($kg\,m^{-2}\,yr^{-1}$)	26.04 (+5.78)	−139 (−17.3)	−44.2 (−12.8)
skin reservoir content (mm)	0.008 (+0.001)	0.005 (−0.002)	−0.016 (−0.003)
snow accumulation over land ($kg\,m^{-2}\,yr^{-1}$)	0.053 (+0.013)	0.192 (+0.255)	0.027 (+0.13)
maximum field capacity of soil (cm)	2.38 (+2.38)	1.89 (−7.05)	−8.76 (−8.34)
total precipitation over land ($kg\,m^{-2}\,yr^{-1}$)	32.5 (+6.9)	142 (−15)	−46.7 (−9.47)
Po-Eo ($kg\,m^{-2}\,yr^{-1}$)	−2.28 (−1.29)	1.03 (−0.12)	0.68 (−0.35)

CPD
9, 2717–2770, 2013

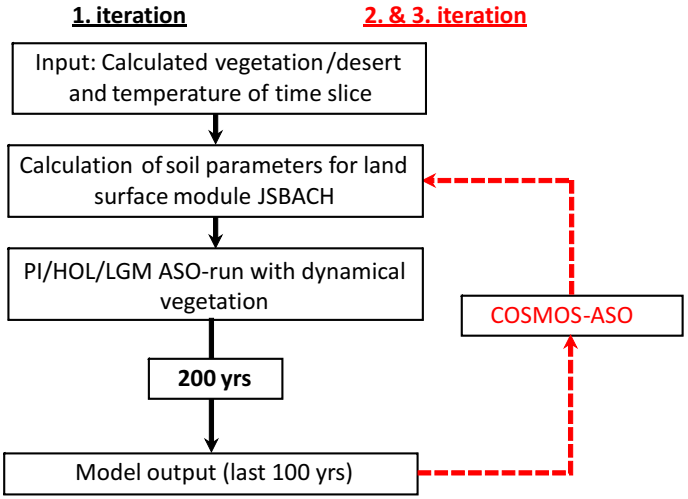

Fig. 1. Flowchart of asynchronous coupling procedure between soil scheme and COSMOS-ASO.

CPD
9, 2717–2770, 2013

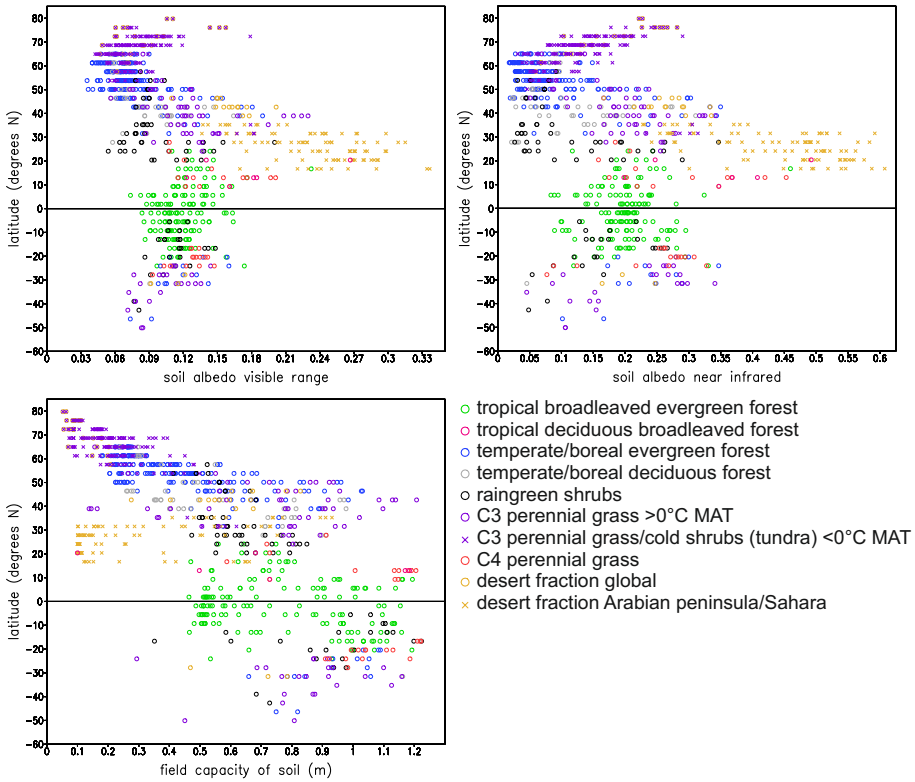

Fig. 2. Physical soil properties (abscissa) used in the dynamical vegetation module JSBACH associated with plant functional types along latitudes. Albedo values are derived from modified satellite measurements of the Moderate Resolution Imaging Spectroradiometer (MODIS) (Rechid et al., 2009) and water holding field capacity of soils are optimized to plant rooting depths (Hagemann et al., 1999).

CPD
9, 2717–2770, 2013

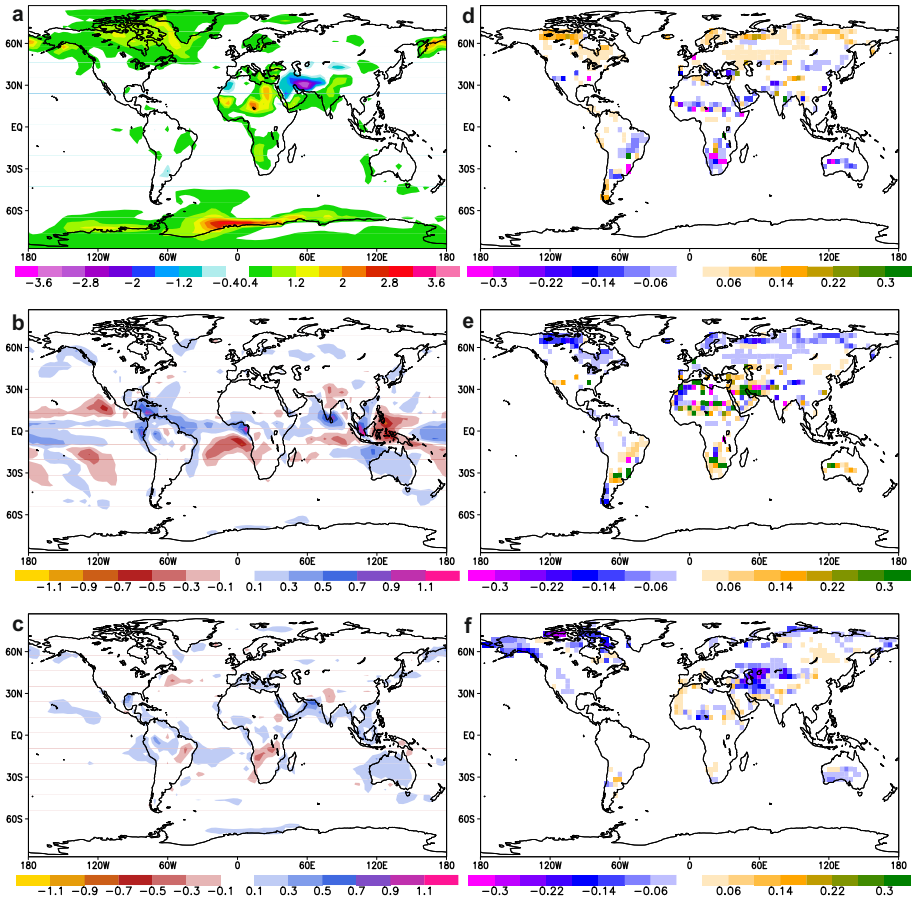

Fig. 3. Differences in 100 yr mean of the pre-industrial climate state with included soil dynamics and fixed soil characteristics (PI_sol-PI_ctl) for **(a)** surface air temperature in °C, **(b)** total precipitation in mm day^{-1}, **(c)** evaporation in kg m^{-2} day^{-1}, **(d)** forest fraction, **(e)** grass fraction and **(f)** desert fraction.

CPD
9, 2717–2770, 2013

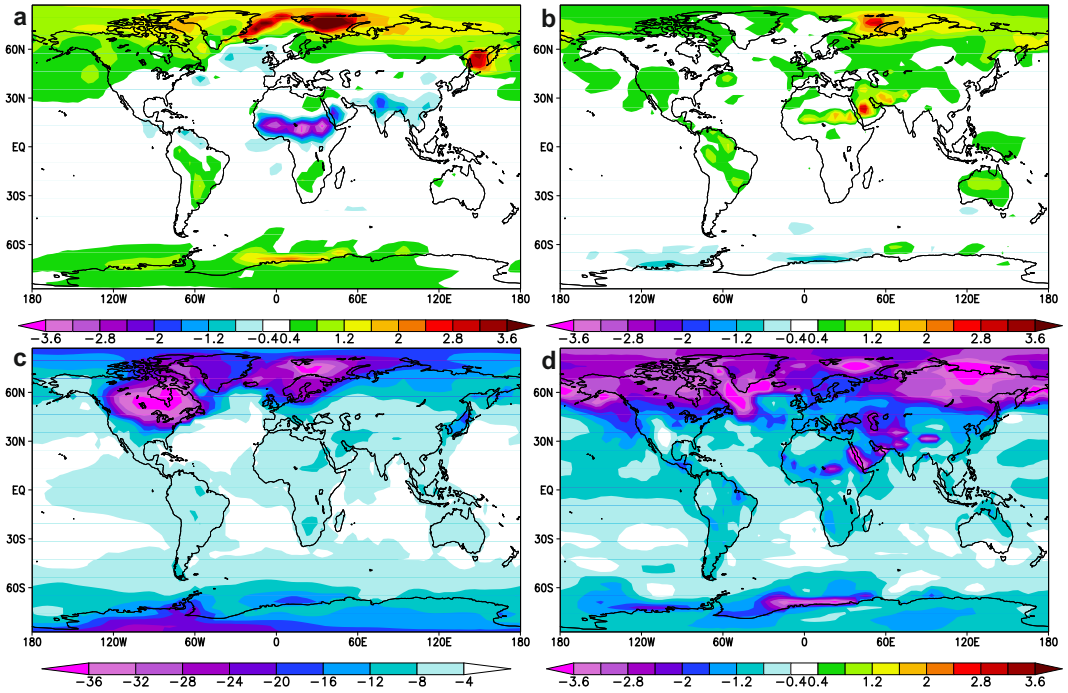

Fig. 4. Surface air temperature (°C) anomalies of a 100 yr mean climate state with respect to Pre-industrial for **(a)** mid-Holocene (HOL_sol-PI_sol), **(b)** mid-Holocene soil feedback ($\widehat{f}_{\mathrm{HOL,sol}}$), **(c)** Last Glacial Maximum (LGM_sol-PI_sol), **(d)** Last Glacial Maximum soil feedback ($\widehat{f}_{\mathrm{LGM,sol}}$).

CPD
9, 2717–2770, 2013

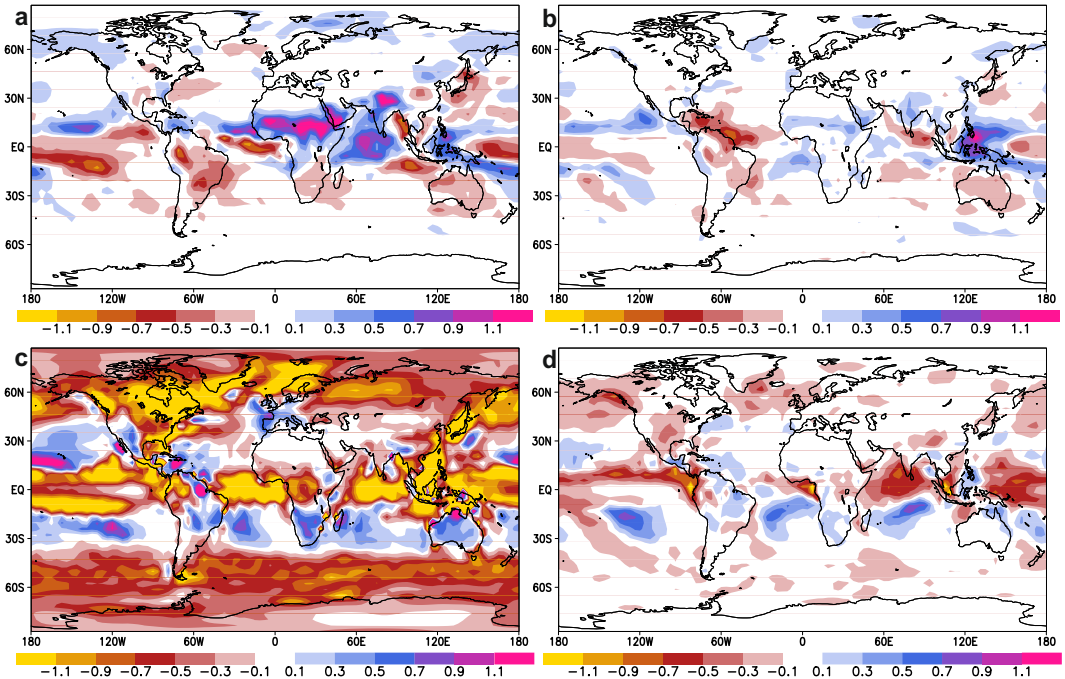

Fig. 5. Total precipitation (mm day^{-1}) anomalies of a 100 yr mean climate state with respect to Pre-industrial for **(a)** mid-Holocene (HOL_sol-PI_sol), **(b)** mid-Holocene soil feedback ($\widehat{f}_{\mathrm{HOL,sol}}$), **(c)** Last Glacial Maximum (LGM_sol-PI_sol), **(d)** Last Glacial Maximum soil feedback ($\widehat{f}_{\mathrm{LGM,sol}}$).

CPD
9, 2717–2770, 2013

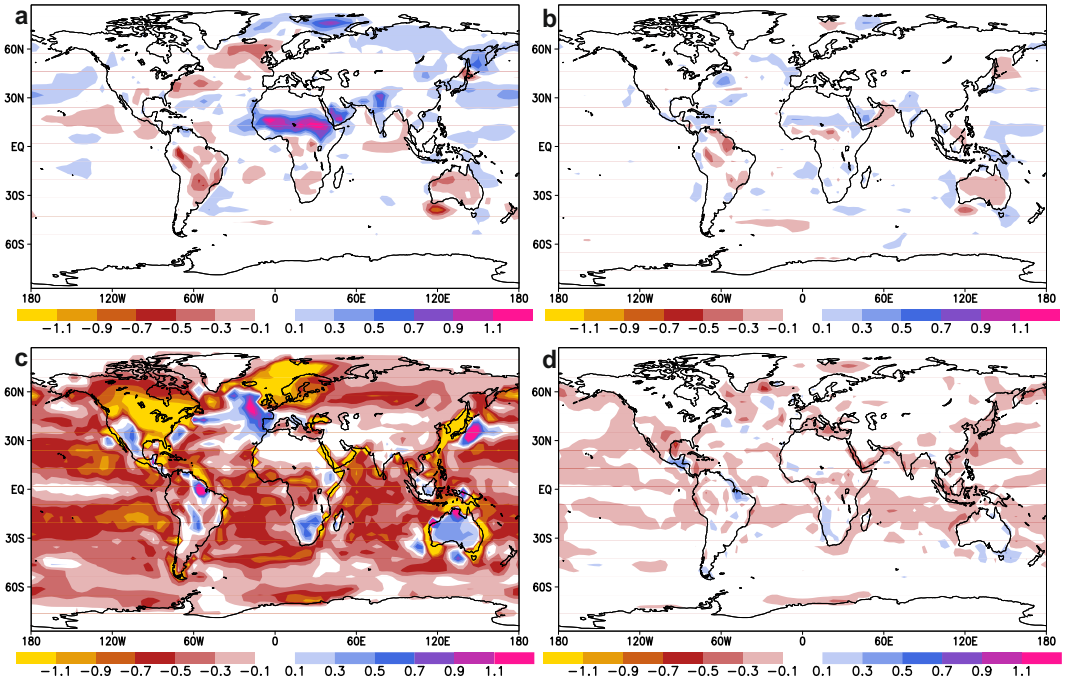

Fig. 6. Evaporation ($kg\,m^{-2}\,day^{-1}$) anomalies of a 100 yr mean climate state with respect to Pre-industrial for **(a)** mid-Holocene (HOL_sol-PI_sol), **(b)** mid-Holocene soil feedback ($\widehat{f}_{HOL,sol}$), **(c)** Last Glacial Maximum (LGM_sol-PI_sol), **(d)** Last Glacial Maximum soil feedback ($\widehat{f}_{LGM,sol}$).

CPD
9, 2717–2770, 2013

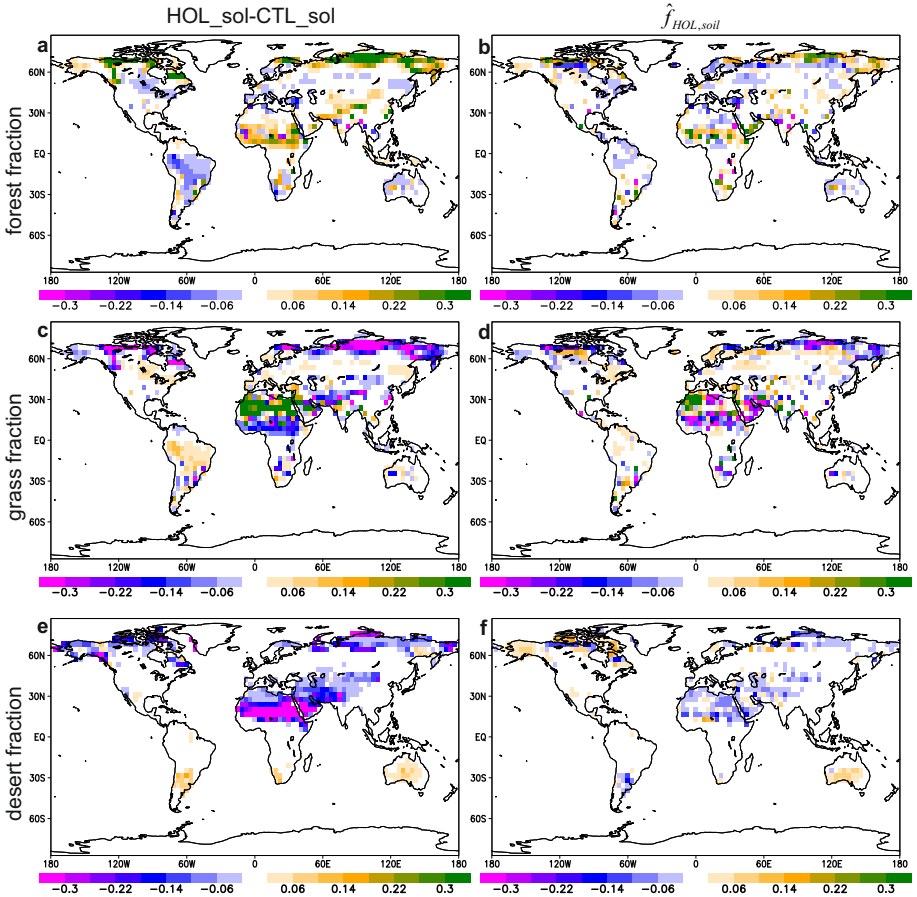

Fig. 7. Vegetation differences in 100 yr mean of the mid-Holocene and pre-industrial climate state with included soil dynamics (HOL_sol-PI_sol) and enclosed soil feedback ($\widehat{f}_{HOL,sol}$), for **(a)** forest fraction and **(b)** soil impact on forest fraction, **(c)** grass fraction and **(d)** soil impact on grass fraction, **(e)** desert fraction and **(f)** soil impact on desert fraction.

CPD
9, 2717–2770, 2013

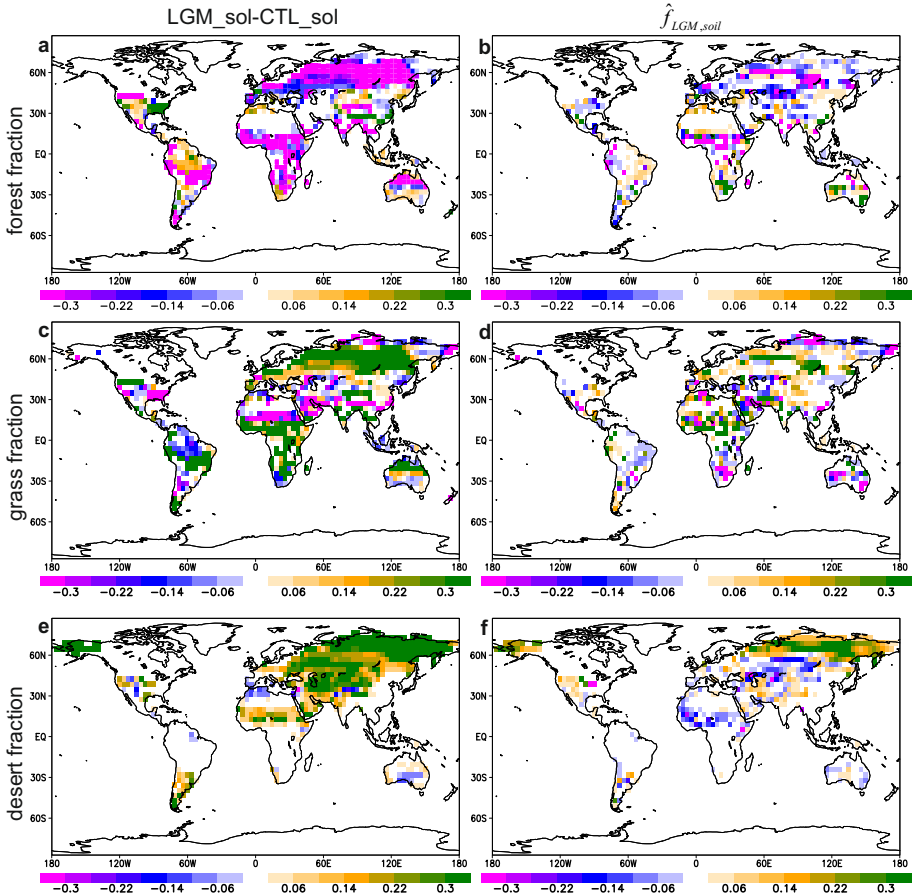

Fig. 8. Vegetation differences in 100 yr mean of the Last Glacial Maximum and Pre-industrial climate state with included soil dynamics (LGM_sol-PI_sol) and enclosed soil feedback ($\hat{f}_{LGM,sol}$), for **(a)** forest fraction and **(b)** soil impact on forest fraction, **(c)** grass fraction and **(d)** soil impact on grass fraction, **(e)** desert fraction and **(f)** soil impact on desert fraction.

CPD
9, 2717–2770, 2013

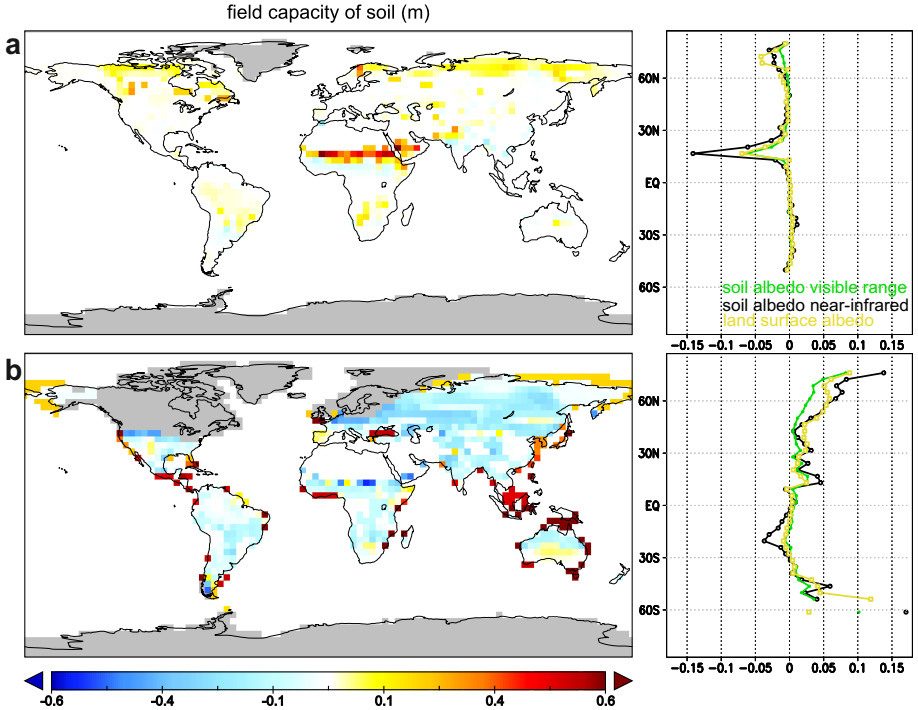

Fig. 9. Changes in water holding field capacities (m) in soils and zonally integrated land surface and soil albedo for **(a)** mid-Holocene (HOL_sol-PI_sol) and **(b)** Last Glacial Maximum (LGM_sol-PI_sol).

CPD
9, 2717–2770, 2013

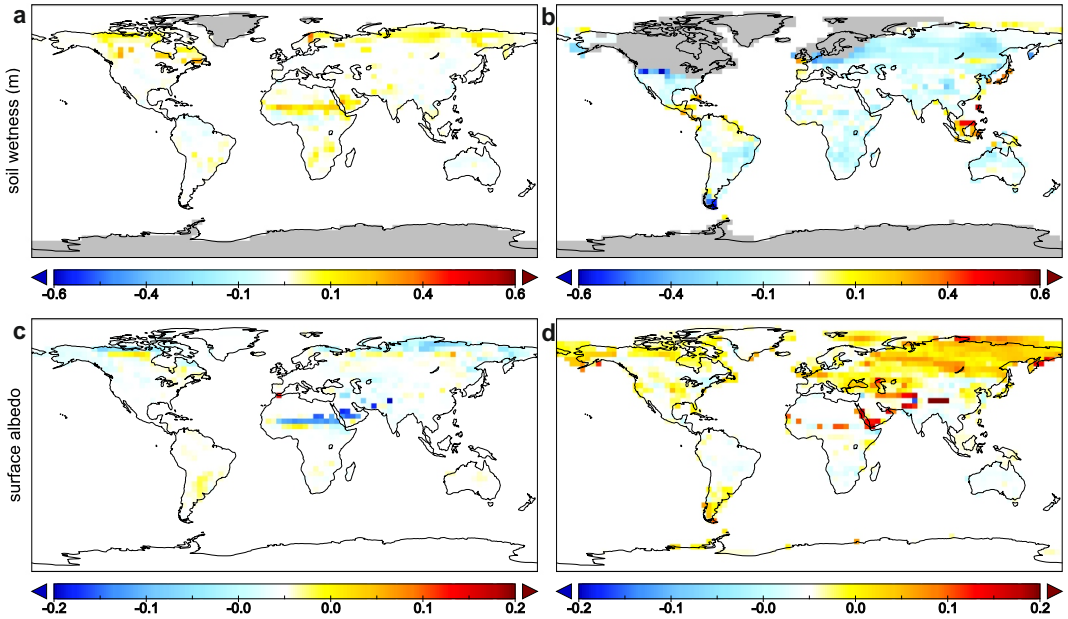

Fig. 10. Soil wetness (m) anomalies of a 100 yr mean climate state with respect to Pre-industrial for **(a)** mid-Holocene (HOL_sol-PI_sol), **(b)** and Last Glacial Maximum (LGM_sol-PI_sol) and changes in surface albedo for **(c)** mid-Holocene and **(d)** Last Glacial Maximum.

CPD
9, 2717–2770, 2013

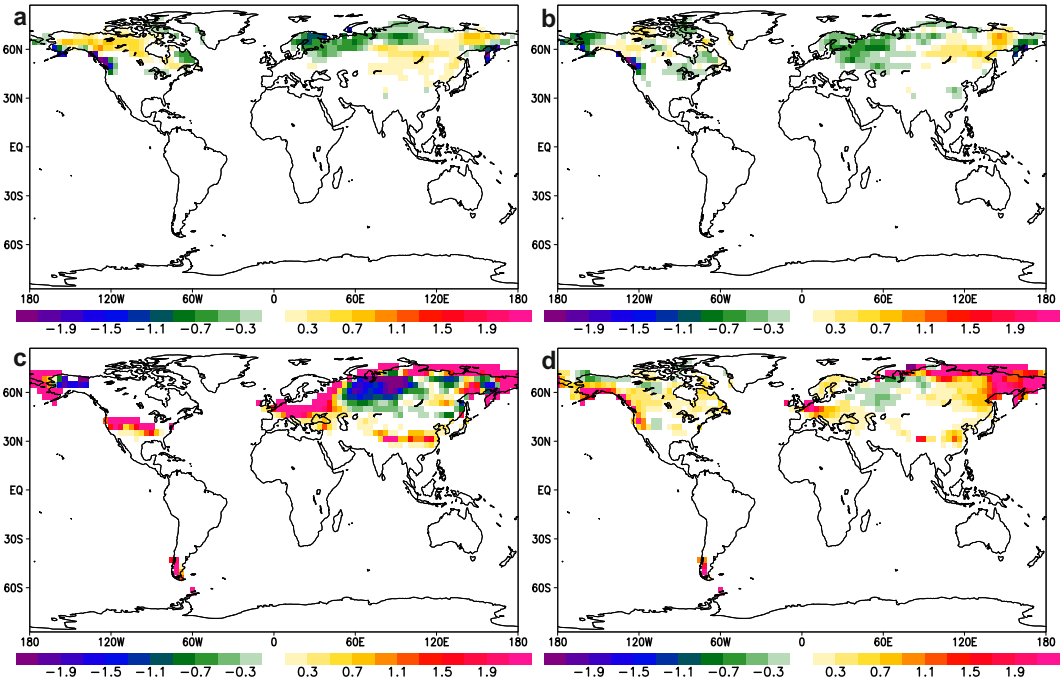

Fig. 11. Snow depth (water equivalent in mm) anomalies of a 100 yr mean climate state with respect to Pre-industrial for **(a)** mid-Holocene (HOL_sol-PI_sol), **(b)** mid-Holocene soil feedback ($\widehat{f}_{\mathrm{HOL,sol}}$), **(c)** Last Glacial Maximum (LGM_sol-PI_sol), **(d)** Last Glacial Maximum soil feedback ($\widehat{f}_{\mathrm{LGM,sol}}$).

CPD
9, 2717–2770, 2013